

FB82-218926

REPORT NO.  
UCB/EERC-82/01  
JANUARY 1982

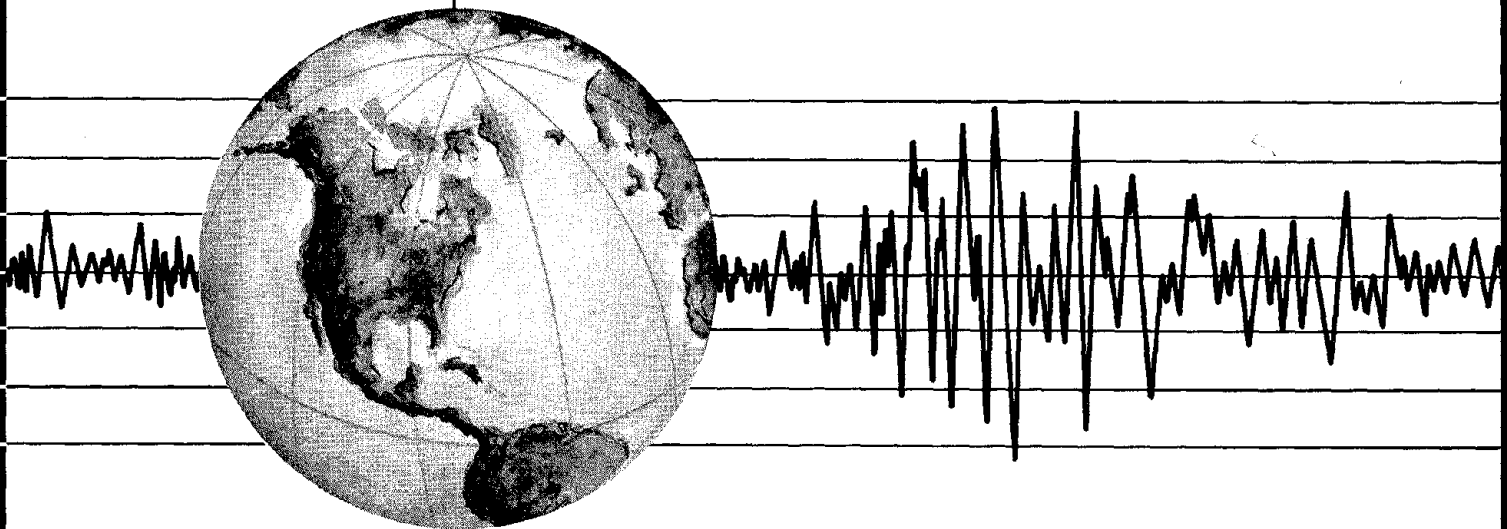
EARTHQUAKE ENGINEERING RESEARCH CENTER

# DYNAMIC BEHAVIOR OF GROUND FOR SEISMIC ANALYSIS OF LIFELINE SYSTEMS

by

TADANOBU SATO  
ARMEN DER KIUREGHIAN

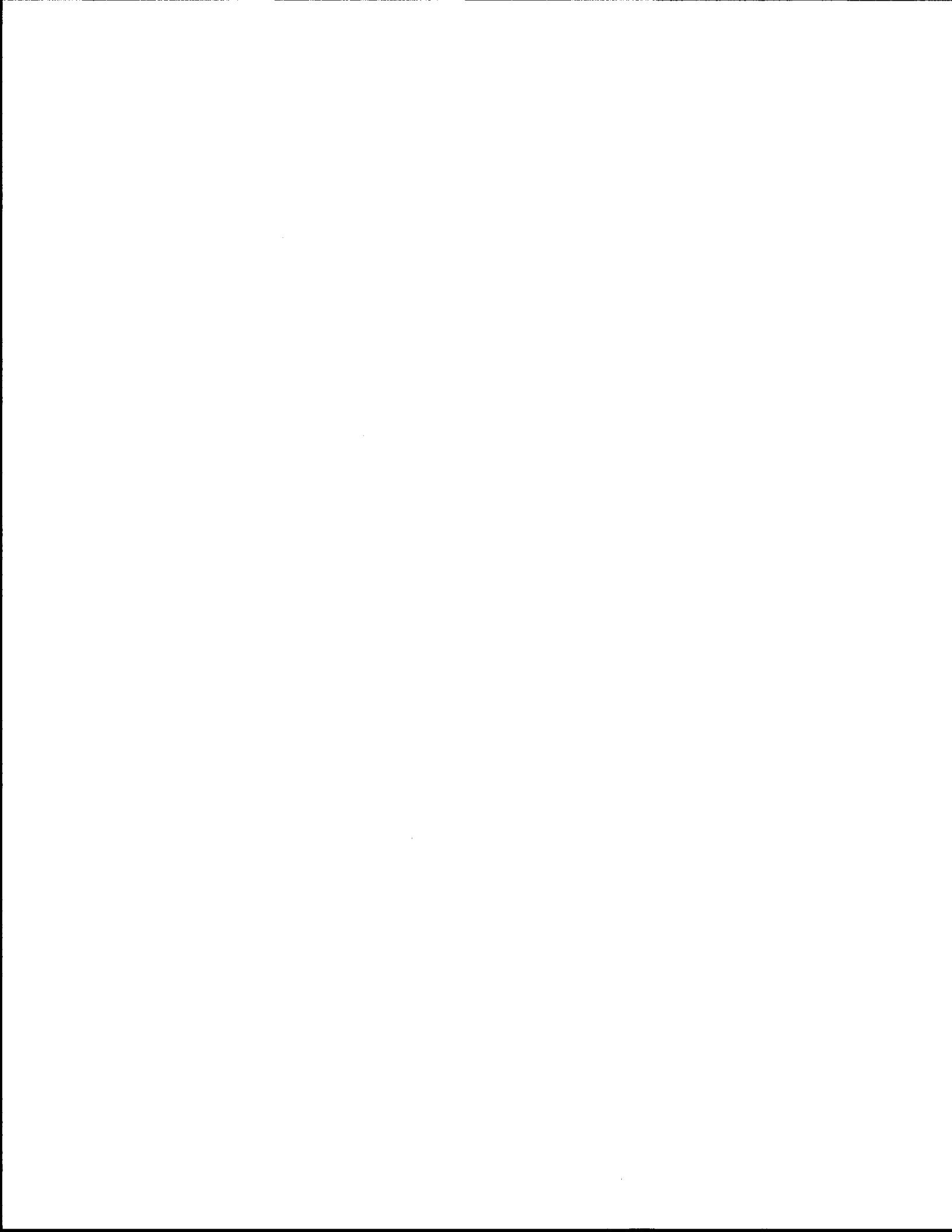
Report to the National Science Foundation



COLLEGE OF ENGINEERING

UNIVERSITY OF CALIFORNIA · Berkeley, California

REPRODUCED BY  
NATIONAL TECHNICAL  
INFORMATION SERVICE  
U.S. DEPARTMENT OF COMMERCE  
SPRINGFIELD, VA 22161



**DYNAMIC BEHAVIOR OF GROUND FOR SEISMIC  
ANALYSIS OF LIFELINE SYSTEMS**

by

Tadanobu Sato  
Visiting Assistant Research Engineer  
University of California, Berkeley  
and  
Associate Professor of Civil Engineering  
Disaster Prevention Research Institute  
Kyoto University, Japan

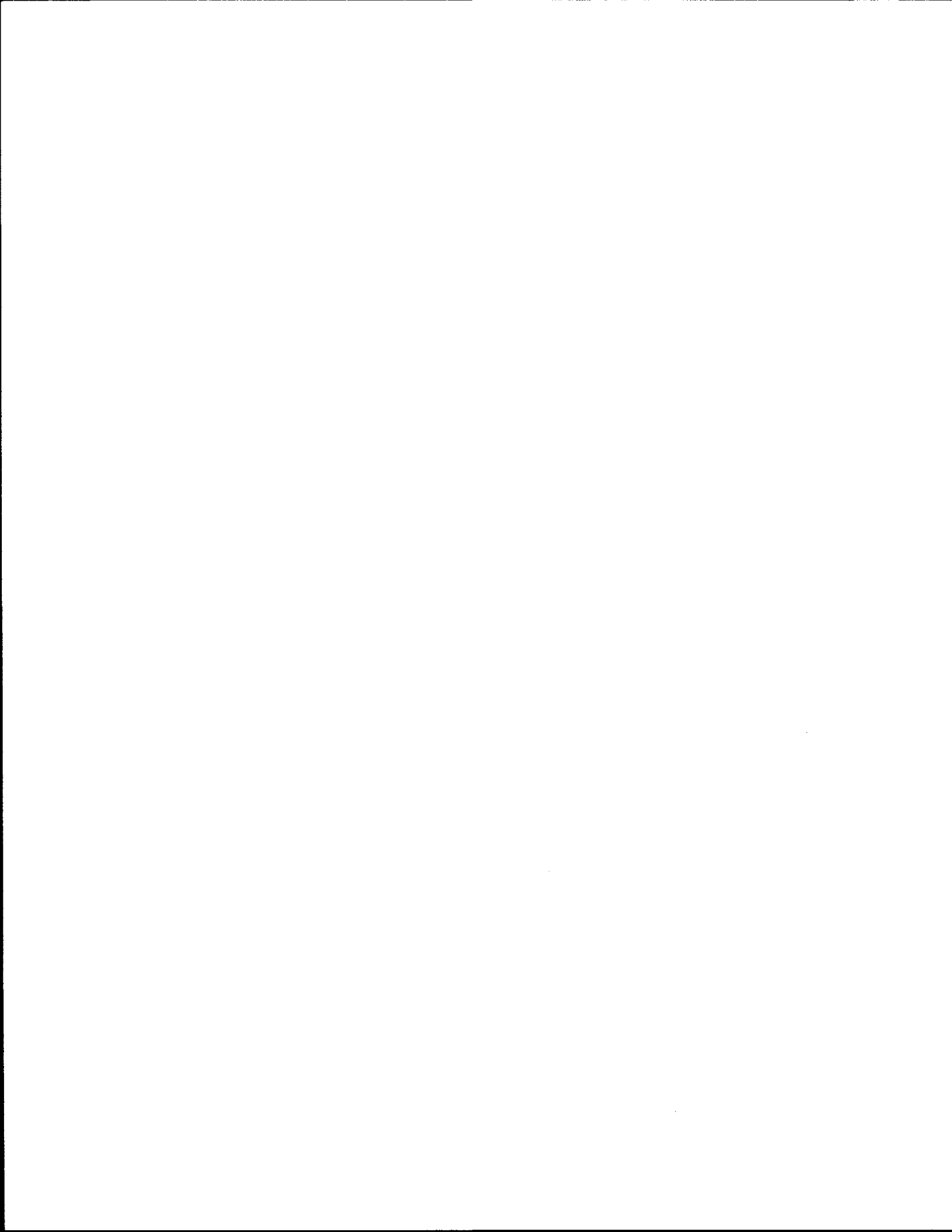
and

Armen Der Kiureghian  
Associate Professor of Civil Engineering  
University of California, Berkeley

A report on research sponsored by  
the National Science Foundation

Report No. UCB/EERC-82/01  
Earthquake Engineering Research Center  
College of Engineering  
University of California, Berkeley

January 1982



#### ACKNOWLEDGEMENT

This research was supported by the National Science Foundation under Grant PFR-7822265 with the University of California, Berkeley.

## ABSTRACT

A new mathematical formula is derived for the general wave transfer function in multi-layered media with inhomogeneous and nonlinear properties of soil. It is assumed that the ground consists of horizontally stratified layers overlying a homogeneous half-space which is excited by vertically incident, plane shear waves. To formulate the nonlinear harmonic wave solution, the surface layer is regarded as a multi-layered system consisting of infinite numbers of sub-layers with infinitesimal thicknesses. To take into account the nonlinearity of the soil element, an equivalent shear modulus and viscosity are used in each sub-layer. By applying the multi-reflection theory to the multi-layered ground, a recurrent-form solution is obtained. Reducing the thickness of each sub-layer to zero, the recurrent-form solution is converted into an integral-form solution.

The mode-superposition procedure based on response spectrum provides an expedient tool for dynamic analysis of surficial ground. The characteristic equation for obtaining natural frequencies and free vibration modes are derived by using the proposed wave transfer function. To use the modal analysis for nonlinear systems, which previously has been used only for linear systems, a repetition scheme for calculating the modal stiffness and damping is proposed which is an adaptation of the equivalent linearization technique. When the energy dissipation of soil is proportional to its shear modulus, the normal mode approach can be performed conveniently by this newly proposed iteration scheme. However, more generally, the equivalent linearized damping matrix is not orthogonal with respect to the undamped mode shapes. In such cases, it is common to ignore off-diagonal terms representing modal coupling. It is shown that this approximation may lead to gross errors, especially when natural frequencies are closely spaced. Here, we propose a new estimator for proportional damping which is based on minimization of mean-square error.

The intensity of ground shaking is estimated based on a response spectrum method for stationary random vibration analysis. Results are given for the stress and stress rate distributions with depth as normalized by the maximum velocity at the ground surface. These response quantities are not significantly affected by either the inhomogeneity or the nonlinearity of the soil layer, or by the epicentral distance of the earthquake. Moreover, the relationship between modal damping and epicentral distances shows that the damping ratio is insensitive to epicentral distances in lower frequency modes. Thus, the assumption of constant strain-independent modal damping is found to be reasonable for practical purposes.

Above results in conjunction with fatigue theory are used to study the liquefaction problem in soil layers with general topography. It is found that the relative density of soil and its effective vertical pressure are important factors in determining liquefaction potential. The next most important term is the shear stress in the soil and the least important is the shear stress rate with time. The ground water level is also found to strongly affect the liquefaction potential.

Application of the proposed methods in seismic reliability assessment of lifeline systems is discussed and several numerical examples are presented. It is shown that the seismic hazard for buried pipes drastically changes in transitional region of the geological structure from shallow to deep soils.

## TABLE OF CONTENTS

	Page
Acknowledgement.....	i
Abstract.....	ii
1. INTRODUCTION.....	1
2. WAVE PROPAGATION THEORY OF LAYERED MEDIA.....	4
2.1 Formulation of the Solution.....	4
2.2 Recurrent Form Solution.....	6
2.3 Integral Form Solution.....	8
3. EVALUATION OF GROUND SHAKING.....	11
3.1 Equivalent Shear Modulus and Damping Factor.....	11
3.2 Natural Frequencies and Free Vibration Modes.....	14
3.3 Orthogonality of Undamped Vibration Mode Shapes.....	16
3.4 The Dynamic Response of Soil Layer.....	18
3.5 Decoupling of Non-linear Damping.....	20
3.6 Determination of Soil Response Based on Response Spectrum.....	21
3.7 Application.....	23
4. ANALYSES OF LIQUEFACTION PHENOMENA.....	40
4.1 S-N Curve for Undrained Saturated Sand.....	40
4.2 Fatigue Theory.....	42
4.3 Application.....	43
5. APPLICATION TO SEISMIC RISK ANALYSIS OF LIFE-LINE SYSTEM.....	47
5.1 The Transition Distance.....	48
5.2 Seismic Risk Potential.....	49
6. CONCLUSION.....	57
Appendix.....	59
REFERENCES.....	61

## 1. INTRODUCTION

To assess the seismic reliability of lifeline systems, the following items should be considered: (i) seismic activity and attenuation of seismic waves, (ii) microzonation with consideration to the local geological nature of each area, (iii) structural response and systems analysis, and (iv) lifeline serviceability requirements. This report relates mainly to the first and second items. The velocity or dynamic strain level in the soil layer during strong earthquakes is a key parameter in the aseismic design of buried structures, especially pipeline systems. In this report, the velocity and strain magnitudes developing in the sub-surface ground during earthquakes are studied by using a non-linear harmonic wave solution, derived theoretically, for infinite inhomogeneous surficial layers with non-linear properties. Another important subject is liquefaction of the soil layer. The fatigue theory is employed to analyze the liquefaction phenomenon of sub-surface ground by considering the stochastic nature of seismic motions.

In the past decade, a large amount of research has been done to construct an unified theory for expressing the field equations of continuous media, i.e., the characteristics of non-linear field equations including their constitutive relationship. Wave propagation in continuous media has been analyzed by many researchers who have used simple wave and discontinuity solutions to study various problems. The state of the art has been surveyed by Chen [1] who has summarized the recent research on discontinuity in non-linear, viscoelastic media. However, these solutions cannot be applied to seismic response analysis of layered ground because the simple wave solution treats only monotonic waves in an infinite space and the solution of discontinuity does not provide any information beyond that of describing the characteristics of the wave front. To evaluate the magnitude of ground shaking during strong earthquakes, it is necessary to develop a solution for non-linear harmonic wave propagation in layered media with repeating reflections and refractions. A solution for non-linear harmonic wave propagation in one direction in a medium with bi-linear hysteresis was developed by Caughey [2] using the slowly varying parameter method. This solution, however, also cannot be applied to cases in which reflecting waves exist.

Techniques used for analyzing the dynamic behaviour of surficial ground during strong earthquakes can be roughly classified into three methods. The first method is to use the multi-reflection theory which is limited to the linear response of the ground. The second more practical method is one in which the soil layer is modeled as a finite system using such spatial and time discretization techniques as the finite element method, the lumped mass method and the finite difference method. The advantage of this second method is that it becomes possible to analyze the seismic response of the ground with non-linear properties. However, in most such analyses, it has been necessary to assume that the base rock is rigid. This makes it difficult to take into account the energy dissipation caused by waves radiating into the underlying half-space. The third method is a combination of the two preceding methods. Since this combined method is based on the wave propagation theory, we can evaluate the effect of energy dissipation for the discretized region, in which the non-linear stress-strain relation is applicable. Although a numerical approach utilizing any integration method in time and space can be used to obtain the seismic response of a surficial ground for any specified time history, in order to achieve an overall understanding of the dynamic behaviour of surficial ground it is essential to develop analytical solutions for non-linear waves.

The important factors governing the mechanical characteristics of soil are the void ratio, the confining pressure, its degree of saturation and the shear wave velocity. In particular, the dynamic behaviour of soil is strongly dependent on the magnitude of shear strain. Soil shows elastic behaviour if the strain level is less than  $10^{-5} \sim 10^{-4}$ . Below this level, the dynamic characteristic of soil can be determined by measuring the modulus of elasticity. If the strain exceeds the above mentioned level, the soil shows dynamic hysteresis. At the strain level of  $10^{-2}$ , the dynamic yield and failure of soil become predominant. A constitutive relationship applicable to the entire range of strain levels has not yet been developed, even though numerous stress-strain relationships based on theories of plasticity, visco-plasticity, elasto-visco-plasticity, and on the micro-structure of soil particle have been proposed by various researchers [3]. Whatever constitutive relationships are used for the seismic response analyses

of surficial ground, it is essential that soil be considered as a non-linear material, especially in the case of strong earthquake motions. At such times, the strain level has been estimated to reach the level of  $10^{-3}$  [4]. A non-linear equation of motion, therefore, is inevitable. An analytical method in wave propagation theory, which makes it possible to evaluate the effect of non-linearity of soil properties, must be developed.

The phenomena of liquefaction of soil has been discussed in many publications after the occurrence of the Nigata Earthquake (1964). The state of the art has been surveyed by Seed [5]. In recent analytical research on liquefaction, the soil is considered as a mixture constructed from separate phases of solid granular skeleton and pore water with certain coupling between the two phases [6-8]. These analyses, however, were based on numerical calculations because constitutive relationships in which the dilatancy phenomena were considered could not be expressed by a linear relationship. On the other hand, the seismic occurrence has a stochastic nature and earthquake wave motions show random characteristics. To include these effects into analyses of liquefaction, more simple but effective methods should be considered. Therefore, a cumulative damage approach based on Miner's law has been utilized. Although the fatigue theory has already been applied to the liquefaction problem by several authors [9-11], in the previous research the actual time history of stress induced in a surficial ground was used. Therefore, it has been difficult to obtain a general understanding of the liquefaction phenomenon considering the stochastic nature of the earthquake motion. To avoid this kind of difficulty, here we have used the stochastic process approach in evaluating the intensity of ground shaking and in calculating the fatigue life.

## 2. WAVE PROPAGATION THEORY OF LAYERED MEDIA

The purpose of this section is to develop a new analytical solution for waves propagating in a vertically inhomogeneous soil layer including the non-linearity in soil properties. It is a well known fact that the incident angle of body waves becomes smaller near the ground surface and an analysis based on the multi-reflection theory gives a good approximation of actual ground motions. In the theory being developed in this paper, it is assumed that the ground consists of horizontally stratified layers overlying homogeneous half-space which is excited by vertically incident, plane shear waves.

### 2.1. Formulation of the Solution

The material characteristics of ground are assumed to be non-linear viscoelastic, in which the shear modulus,  $\mu$ , and the shear viscosity,  $\nu$ , are expressed as functions of depth,  $z$ , and strain magnitude,  $\gamma_0(z)$ , i.e.,

$$\mu = \mu(\gamma_0, z), \quad \nu = \nu(\gamma_0, z). \quad (2.1)$$

The well known field equation is given by

$$\rho \frac{\partial^2 u}{\partial t^2} = \frac{\partial}{\partial z} \left( \mu \frac{\partial u}{\partial z} + \nu \frac{\partial^2 u}{\partial t \partial z} \right) \quad (2.2)$$

where  $\rho(z)$  is the soil density,  $u(z, t)$  is the horizontal displacement, and  $t$  is the time. When a wave with random nature propagates in a layered medium, the value of  $\gamma_0$  cannot be determined unconditionally. This value, however, may be chosen for the peak strain amplitude in the case of non-linear harmonic wave propagation with constant amplitude. A detailed discussion of this point is given in the next section.

To formulate the non-linear harmonic wave solution, the surface layer is regarded as a kind of multi-layered system consisting of infinite numbers of sub-layers with infinitesimal thicknesses as shown in Figure 2.1. It is assumed that  $\mu$  and  $\nu$  have constant values in each sub-layer. Although  $\mu$  and  $\nu$  are functions of  $z$  and  $\gamma_0(z)$ , this assumption is made possible by replacing  $\mu$  and  $\nu$  with  $\mu_j$  and  $\nu_j$  which are representative values in the  $j$ th sub-layer. By applying the multi-reflection theory to this kind of multi-layered ground, a recurrent form

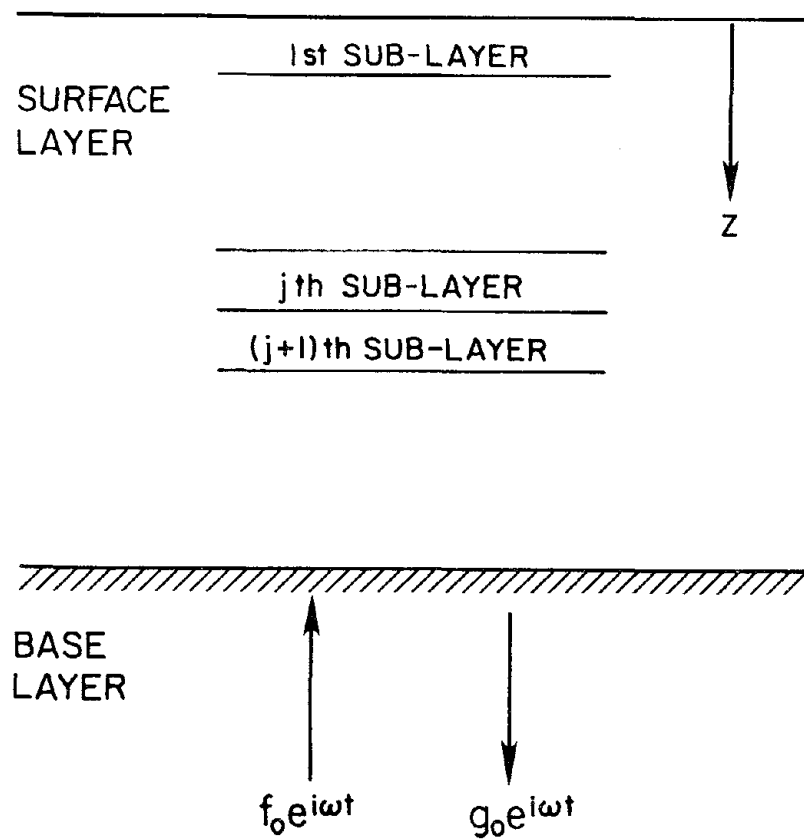


**Figure 2.1** Soil layer modeled as multiple sublayers

solution is obtained. Reducing the thickness of each sub-layer to zero, the recurrent form solution is reduced to an integral form solution.

## 2.2. Recurrent Form Solution

Based on the assumption of constant  $\mu$  and  $\nu$  in each sub-layer, Equation (2.2) for the  $j$ th layer reduces to a linear equation for vertically propagating shear waves

$$\rho_j \frac{\partial^2 u_j}{\partial t^2} = \mu_j \frac{\partial^2 u_j}{\partial z_j^2} + \nu_j \frac{\partial^3 u_j}{\partial t \partial z_j^2} \quad (2.3)$$

where  $\rho_j$ ,  $u_j$  and  $z_j$  are the soil density, horizontal displacement and coordinate of the  $j$ th sub-layer, respectively.

Harmonic displacement with frequency  $\omega$  can be written in the form

$$u_j(z_j, t) = U(z_j) e^{i\omega t} \quad (2.4)$$

Substituting Equation (2.4) in Equation (2.3) results in an ordinary differential equation

$$(\mu_j + i\omega\nu_j) \frac{d^2 U_j}{dz_j^2} + \rho_j \omega^2 U_j = 0 \quad (2.5)$$

The general solution of Equation (2.5) is given by

$$U_j(z_j) = a_j \exp(ip_j z_j) + b_j \exp(-ip_j z_j) \quad (2.6)$$

where

$$p_j^2 = \rho_j \omega^2 / (\mu_j + i\omega\nu_j) \quad (2.7)$$

where  $i = \sqrt{-1}$ ,  $a_j$  and  $b_j$  are arbitrary constants. The following equation is obtained from the boundary condition at the interface between the  $j$ th and  $(j-1)$ th sub-layers.

$$\begin{pmatrix} a_j \\ b_j \end{pmatrix} = [t_{j-1}] \begin{pmatrix} a_{j-1} \\ b_{j-1} \end{pmatrix} \quad (2.8)$$

where

$$[t_j] = \begin{bmatrix} \xi_j \exp(ip_j h_j) & \eta_j \exp(-ip_j h_j) \\ \eta_j \exp(ip_j h_j) & \xi_j \exp(-ip_j h_j) \end{bmatrix} \quad (2.9)$$

in which

$$\xi_j = \frac{1}{2} \left[ 1 + \frac{\beta_j}{\beta_{j+1}} \right] \quad (2.10a)$$

$$\eta_j = \frac{1}{2} \left[ 1 - \frac{\beta_j}{\beta_{j+1}} \right] \quad (2.10b)$$

$$\beta_j = \frac{p_j}{\omega} (\mu_j + i\omega\nu_j) . \quad (2.10c)$$

By repeating Equation (2.8), the following relation is obtained

$$\begin{bmatrix} a_j \\ b_j \end{bmatrix} = [T] \begin{bmatrix} a_1 \\ b_1 \end{bmatrix} \quad (2.11a)$$

where

$$[T] = [t_{j-1}][t_{j-2}] \cdots [t_2][t_1] . \quad (2.11b)$$

Substituting  $[t_j]$  from Equation (2.9) in Equations (2.11) and rearranging in the order of  $\eta_j$ 's power, the recurrent form of the matrix  $[T]$  is obtained as follows

$$\begin{aligned} T_{11} = & \prod_{q=1}^j \xi_q \exp \left\{ i \sum_{l=1}^j p_l h_l \right\} + \sum_{r=1}^{j-1} \eta_r \sum_{k=r+1}^j \eta_k \prod_{q=1}^{r-1} \xi_q \prod_{q=r+1}^{k-1} \xi_q \prod_{q=k+1}^j \xi_q \\ & \cdot \exp \left\{ i \left( \sum_{l=1}^j p_l h_l - 2 \sum_{l=1}^k p_l h_l + 2 \sum_{l=1}^r p_l h_l \right) \right\} \\ & + \sum_{r=1}^{j-3} \eta_r \sum_{k=r+1}^{j-2} \eta_k \sum_{m=k+1}^{j-1} \eta_m \sum_{n=m+1}^j \eta_n \prod_{q=1}^{r-1} \xi_q \prod_{q=r+1}^{k-1} \xi_q \prod_{q=k+1}^{m-1} \xi_q \prod_{q=m+1}^{n-1} \xi_q \prod_{q=n+1}^j \xi_q \\ & \cdot \exp \left\{ i \left( \sum_{l=1}^j p_l h_l - 2 \sum_{l=1}^k p_l h_l + 2 \sum_{l=1}^m p_l h_l - 2 \sum_{l=1}^n p_l h_l \right) \right\} + \cdots . \end{aligned} \quad (2.12a)$$

$$\begin{aligned} T_{12} = & \sum_{r=1}^j \eta_r \prod_{q=1}^{r-1} \xi_q \prod_{q=r+1}^j \xi_q \exp \left\{ i \left( \sum_{l=1}^j p_l h_l - 2 \sum_{l=1}^r p_l h_l \right) \right\} \\ & + \sum_{r=1}^{j-2} \eta_r \sum_{k=r+1}^{j-1} \eta_k \sum_{m=k+1}^j \eta_m \prod_{q=1}^{r-1} \xi_q \prod_{q=r+1}^{k-1} \xi_q \prod_{q=k+1}^{m-1} \xi_q \prod_{q=m+1}^j \xi_q \\ & \cdot \exp \left\{ i \left( \sum_{l=1}^j p_l h_l - 2 \sum_{l=1}^k p_l h_l + 2 \sum_{l=1}^m p_l h_l \right) \right\} + \cdots . \end{aligned} \quad (2.12b)$$

$T_{21}$  and  $T_{22}$  have the same forms as  $T_{12}$  and  $T_{11}$  respectively, except for the signs of the exponential terms which are reversed. From definition of  $\xi_j$  and  $\eta_j$  given by Equations (2.10),  $\xi_j$  and  $\eta_j$  approach unity and zero, respectively, as the thickness of  $j$ th sublayer goes to zero. It appears, therefore, that as an approximation, higher-order terms involving powers of  $\eta_j$  can be neglected. For example, it may be possible for certain cases (as it will be shown later) to only retain the first-order terms, i.e.,  $T_{11} = \sum_{q=1}^j \dots$  and  $T_{12} = 0$ . In general, however, one may retain terms involving higher-order powers of  $\eta_j$  up to any level of accuracy desired.

From Equation (2.6), harmonic displacement  $U_j$  and shear stress  $\tau_j$  at the top of the  $j$ th sub-layer are given as follows

$$U_j = (T_{11} + T_{21})a_1 + (T_{12} + T_{22})b_1 \quad (2.13a)$$

$$\tau_j = i\omega\beta_j(T_{11} - T_{21})a_1 - i\omega\beta_j(T_{22} - T_{12})b_1. \quad (2.13b)$$

### 2.3. Integral Form Solution

If the thickness of the  $j$ th sub-layer goes to zero, the term  $\sum_{l=1}^j p_l h_l$  becomes an integral,

$\int_0^z p(w) dw$ . Then, Equations (2.12) can be rewritten as follows

$$\begin{aligned} T_{11} = \lambda(z) & \left[ \exp \left( i \int_0^z p dw \right) + \int_0^z \kappa(x_2) \int_{x_2}^z \kappa(x_1) \exp \left( i \int_0^z p dw - 2i \int_0^{x_1} p dw + 2i \int_0^{x_2} p dw \right) dx_1 dx_2 \right. \\ & + \int_0^z \kappa(x_4) \int_{x_4}^z \kappa(x_3) \int_{x_3}^z \kappa(x_2) \int_{x_2}^z \kappa(x_1) \exp \left( i \int_0^z p dw - 2i \int_0^{x_1} p dw + 2i \int_0^{x_2} p dw \right. \\ & \left. \left. - 2i \int_0^{x_3} p dw + 2i \int_0^{x_4} p dw \right) dx_1 dx_2 dx_3 dx_4 + \dots \right] \quad (2.14a) \end{aligned}$$

$$\begin{aligned} T_{12} = \lambda(z) & \left[ \int_0^z \kappa(x_1) \exp \left( i \int_0^z p dw - 2i \int_{x_1}^z p dw \right) dx_1 + \int_0^z \kappa(x_3) \int_{x_3}^z \kappa(x_2) \int_{x_2}^z \kappa(x_1) \right. \\ & \left. \cdot \exp \left( i \int_0^z p dw - 2i \int_0^{x_1} p dw + 2i \int_0^{x_2} p dw - 2i \int_0^{x_3} p dw \right) dx_1 dx_2 dx_3 + \dots \right] \quad (2.14b) \end{aligned}$$

$T_{21}(z)$  and  $T_{22}(z)$  have the same forms as  $T_{12}(z)$  and  $T_{11}(z)$ , respectively, except that the signs of the exponential terms are reversed. In these expressions,  $\lambda(z)$  and  $\kappa(z)$  are derived from the infinite product  $\lim_{h_k \rightarrow 0} \prod_{k=1}^{j-1} \xi_k$  and from  $\lim_{h_k \rightarrow 0} \eta_k$ , respectively. Here, the method for obtaining the following results is shown in Appendix 1:

$$\lambda(z) = \left\{ \frac{\beta(0)}{\beta(z)} \right\}^{1/2}, \quad (2.15)$$

$$\kappa(z) = \frac{1}{2\beta(z)} \frac{d\beta(z)}{dz} \quad (2.16)$$

where

$$\beta(z) = \frac{p(z)}{\omega} \left\{ \mu(z, \gamma_0) + i\omega\nu(z, \gamma_0) \right\} \quad (2.17)$$

$$p^2(z) = \frac{\rho(z)\omega^2}{\{\mu(z, \gamma_0) + i\omega\nu(z, \gamma_0)\}} \quad (2.18)$$

The harmonic displacement and shear stress given by Equation (2.13) are also transformed as functions of depth  $z$

$$U(z) = \{T_{11}(z) + T_{12}(z)\}A + \{T_{12}(z) + T_{22}(z)\}B \quad (2.19a)$$

$$\tau(z) = i\omega\beta(z)\{T_{11}(z) - T_{21}(z)\}A - i\omega\beta(z)\{T_{22}(z) - T_{12}(z)\}B \quad (2.19b)$$

where  $A$  and  $B$  are arbitrary coefficients defined from the boundary condition. A set of simpler expressions for the above solutions is as follows

$$U(z) = f(z)C + g(z)D \quad (2.20a)$$

$$\tau(z) = -\beta(z)\omega g^*(z)C + \beta(z)\omega f^*(z)D \quad (2.20b)$$

where  $C$  and  $D$  are arbitrary constants and  $f(z)$ ,  $g(z)$ ,  $f^*(z)$  and  $g^*(z)$  are derived by expressing the exponential terms in terms of sines and cosines:

$$f(z) = \lambda(z) \left\{ \cos \left[ \int_0^z pdw \right] + \int_0^z \kappa(x_1) \cos \left[ \int_0^z pdw - 2 \int_0^{x_1} pdw \right] dx_1 + \dots \right\} \quad (2.21a)$$

$$g(z) = \lambda(z) \left\{ \sin \left[ \int_0^z pdw \right] - \int_0^z \kappa(x_1) \sin \left[ \int_0^z pdw - 2 \int_0^{x_1} pdw \right] dx_1 + \dots \right\} \quad (2.21b)$$

$$f^*(z) = \lambda(z) \left\{ \cos \left[ \int_0^z pdw \right] - \int_0^z \kappa(x_1) \cos \left[ \int_0^z pdw - 2 \int_0^{x_1} pdw \right] dx_1 + \dots \right\} \quad (2.21c)$$

$$g^*(z) = \lambda(z) \left\{ \sin \left[ \int_0^z pdw \right] + \int_0^z \kappa(x_1) \sin \left[ \int_0^z pdw - 2 \int_0^{x_1} pdw \right] dx_1 + \dots \right\} \quad (2.21d)$$

Note that the minus sign in front of  $\kappa$ 's power in functions  $g(z)$  and  $f^*(z)$  appears in every odd term of  $\kappa$ 's power.

For convenience of treating the boundary conditions, Equations (2.20) are expressed in the form of a transfer matrix as follows

$$\begin{Bmatrix} U(z) \\ \tau(z) \end{Bmatrix} = \begin{bmatrix} f(z) & \frac{g(z)}{\beta(0)\omega} \\ -\beta(z)\omega g^*(z) & \frac{\beta(z)f^*(z)}{\beta(0)} \end{bmatrix} \begin{Bmatrix} U(0) \\ \tau(0) \end{Bmatrix} \quad (2.22)$$

Let us consider the case of a single surface layer overlying homogeneous base layer. At the ground surface shear stress must be zero; then we have

$$U(z) = f(z)U(0) \quad (2.23a)$$

$$\tau(z) = -\beta(z)\omega g^*(z)U(0) \quad (2.23b)$$

When a vertically propagating wave is given as  $f_0 \exp(i\omega t)$  at the top of the base layer, the expression of  $U(0)$  is determined from the boundary condition at an interface between surface and base layer

$$U(0) = \frac{2f_0}{f(H) + i \frac{\beta(H)}{\beta_b(0)} g^*(H)} \quad (2.14)$$

where  $H$  is the depth of surface layer and  $\beta_b(0)$  is the value of  $\beta$  at the top of the base layer.

Though the non-linear harmonic wave solution is expressed as described above, the functions  $f$ ,  $f^*$ ,  $g$  and  $g^*$  given by Equations (2.21) are complex functions of  $\beta(z)$  and  $p(z)$ , and these values are in turn functions of  $\gamma_0(z)$  as apparent from Equations (2.17) and (2.18). Thus, the integrations in Equations (2.21) cannot be done directly. An iterative solution is, therefore, necessary. For this purpose,  $\gamma_0(z)$  is estimated from the linear solution at the beginning of computation. Using this value, the first approximation of  $\beta(z)$  and  $p(z)$  are calculated. Substituting these values in Equations (2.21), the numerical integration of this equation is performed based on a suitable numerical integration method and thus the second estimation of  $\gamma_0(z)$  is obtained. This process is repeated until the computed  $\gamma_0(z)$  converges up to a desired level of accuracy.

### 3. EVALUATION OF GROUND SHAKING

In the preceding discussion of the wave propagation theory, the harmonic displacement of the soil layer was obtained as a function of the depth and strain level. Based on these results, a mode-superposition procedure is developed which provides an expedient tool in cases in which the stochastic dynamic response of surficial ground is required. In this section, the characteristic equation for obtaining the natural frequencies and undamped mode shapes are derived for a layered medium with general inhomogeneous and non-linear properties. The intensity of ground shaking is estimated based on a response spectrum method for stationary random vibration analysis [12]. To use the modal approach for a non-linear system, which has previously been used only for linear systems, an iteration scheme to calculate the modal stiffness and damping are proposed which is an adaptation of the well known equivalent linearization technique. If the energy dissipation of soil is proportional to its shear modulus, the normal mode approach can be expediently performed by this newly proposed iteration scheme. However, for a general case, the damping matrix obtained through equivalent linearization is not orthogonal with respect to the undamped mode shapes and the normal coordinates can not be decoupled. The most commonly used approach is to ignore the off-diagonal terms representing modal coupling. This assumption is reasonable for a system with well spaced natural frequencies. However, in the case of a system with closely spaced modes, this assumption may give a lower estimation of modal damping. Here, we propose a new estimator for equivalent modal damping which is based on concepts of random vibration and includes the effect of closely spaced modes.

#### 3.1. Equivalent Shear Modulus and Damping Factor

A typical stress-strain curve of a soil specimen subjected to cyclic shearing force is shown schematically in Figure 3.1. For the strain amplitude  $\gamma_0$ , the equivalent shear modulus,  $\mu$ , is determined by the slope of line OA, and the equivalent viscous damping factor,  $\zeta$ , is given by the expression

$$\zeta = \frac{1}{2\pi} \frac{\Delta W}{W} \quad (3.1)$$

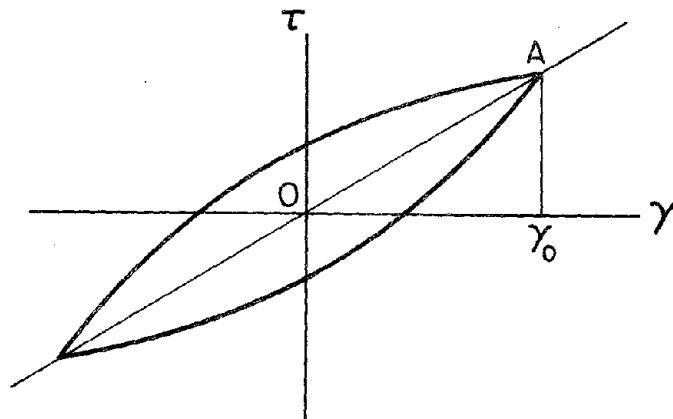


Figure 3.1 Typical stress-strain curve for soil specimen subjected to cyclic loading

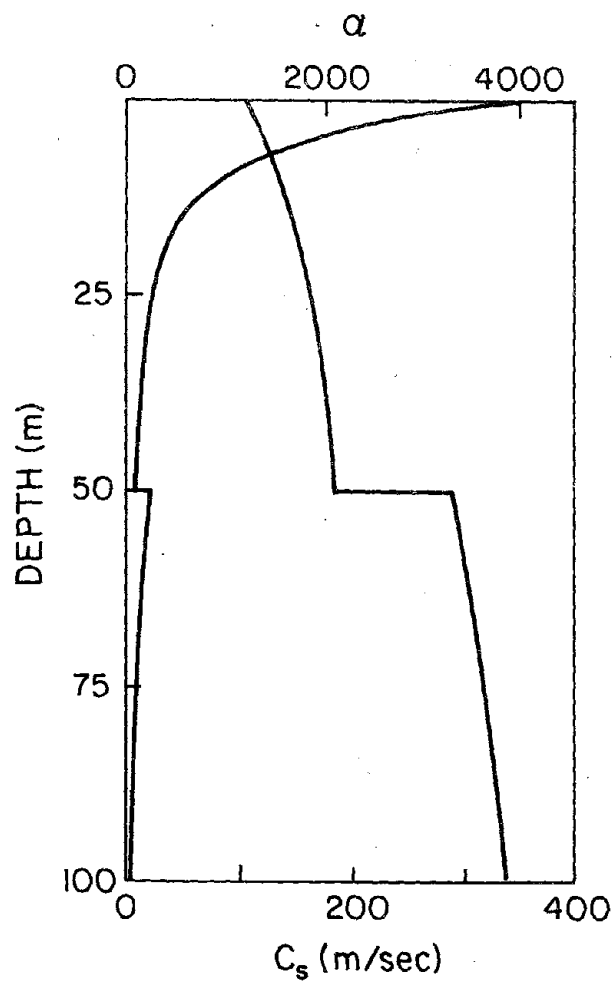


Figure 3.2 Distributions of nonlinearity parameter,  $\alpha$ , and shear wave velocity,  $c_s$

where  $\Delta W$  is the energy loss per cycle and  $W$  is the work done by the applied load. Once the equivalent shear modulus,  $\mu$ , and viscosity,  $\nu$ , are given, the following relationship among  $\zeta$ ,  $\mu$  and  $\nu$  can be used

$$\zeta = \frac{1}{2} \frac{\omega \nu}{\mu} \quad (3.2)$$

where  $\omega$  is the circular frequency.  $\omega$  can be chosen as the excitation frequency provided the applied force is harmonic; however, during random excitation the measure of  $\omega$  should be chosen as the response mean frequency.

Hardin and Drenovich [13] have proposed the following simple mathematical formulae for  $\mu$  and  $\zeta$  based on cyclic torsional shear tests of soil samples:

$$\frac{\mu}{\mu_1} = \frac{1}{1 + \alpha \gamma_0} \quad (3.3)$$

$$\frac{\zeta}{\zeta_m} = \frac{\alpha \gamma_0}{1 + \alpha \gamma_0} \quad (3.4)$$

where  $\mu_1$  is an initial shear modulus,  $\zeta_m$  is a maximum damping factor of the system defined at the infinite shear strain amplitude, and  $\alpha$  is a parameter expressing the degree of non-linearity.

This value can be determined from

$$\alpha = \frac{\mu_1}{\tau_f} \quad (3.5)$$

where  $\tau_f$  is the geostatic shear strength of soil which is defined by

$$\tau_f = \left\{ \left[ c' \cos \phi' + \frac{1 + K_0}{2} \sigma' \sin \phi' \right]^2 - \left[ \frac{1 - K_0}{2} \sigma' \right]^2 \right\}^{1/2} \quad (3.6)$$

where  $c'$  and  $\phi'$  are geostatical strength parameters of soil,  $K_0$  is the coefficient of lateral stress at rest and  $\sigma'$  is the vertically effective overburden pressure. The initial shear modulus is determined from the shear wave velocity,  $c_s$ , at the infinitesimal strain level using the relationship  $\mu_1 = \rho c_s^2$ , where  $\rho$  is the density. The stress dependency of the shear wave velocity is assumed as follows:

$$c_s = D(\sigma' + a)^{1/4} \quad (3.7)$$

where  $D$  and  $a$  are experimental constants of the soil.

### 3.2. Natural Frequencies and Undamped Vibration Modes

The geological topography of actual ground is a stack of inhomogeneous layers with non-linear properties. Therefore, the ground should be treated as a multi-layered system. However, the essential physical characteristics of the vibration modes are easily understood when a single-layered system is considered. Here we first give a detailed discussion of natural frequencies and mode shapes for a single-layered system and then describe how it is extended to multi-layered systems. The displacement and stress in a layer are expressed by the transfer matrix given in Equation (2.22) as follows:

$$\begin{Bmatrix} U(z) \\ \tau(z) \end{Bmatrix} = [A(z, \omega)] \begin{Bmatrix} U(0) \\ 0 \end{Bmatrix} \quad (3.8a)$$

$$A(z, \omega) = \begin{bmatrix} f(z, \omega) & \frac{g(z, \omega)}{\beta(0, \omega)\omega} \\ -\beta(z, \omega)\omega g^*(z, \omega) & \frac{\beta(z, \omega)f^*(z, \omega)}{\beta(0, \omega)} \end{bmatrix} \quad (3.8b)$$

In derivation of Equations (3.8), a stress free condition at ground surface is used. The eigenvalues  $\omega_n$  of the system expressed by Equations (3.8) are given by the characteristic equation

$$U(H, \omega_n) = 0 \quad (n = 1, 2, \dots, \infty). \quad (3.9)$$

The eigenfunction  $\psi_n$  for each eigenvalue is a function of  $z$  and  $\omega_n$ .

$$\psi_n(z, \omega_n) = U(z) |_{U(0)=1} = f(z, \omega_n). \quad (3.10)$$

As indicated before, the functions  $f$ ,  $g$ ,  $f^*$  and  $g^*$  which appear in Equations (2.22) are generally complex-valued functions because  $p(z)$  and  $\beta(z)$  given by Equations (2.17) and (2.18) are complex-valued combinations of the shear modulus and the shear viscosity. Therefore, the eigenvalue,  $\omega_n$ , and the eigenfunction,  $\psi_n$ , are generally complex-valued. When the undamped system, which means  $\nu(z) \equiv 0$ , is considered, the functions  $f$ ,  $g$ ,  $f^*$  and  $g^*$  become real functions. The characteristic equation, Equation (3.9), then gives a real eigenvalue which is usually called the natural frequency. The eigenfunction  $\psi_n$  also becomes a real function which defines the undamped vibration mode of the continuous system.

To make this argument more clear, let us consider the special case of neglecting all the  $\kappa$ 's power terms. Referring to Equation (2.21a), the function  $f(z, \omega)$  is then expressed as

$$f(z, \omega) = \lambda(z, \omega) \cos \left\{ \int_0^z p(\omega, x) dx \right\} \quad (3.11)$$

where

$$p(\omega, x) = \sqrt{\frac{\rho(x)\omega^2}{\mu(z) + i\omega\nu(z)}} \quad (3.12)$$

Substituting  $\omega = \omega_r + i\omega_i$  into Equation (3.12) and considering the characteristic Equation (3.9), the following equations are obtained to determine the real and imaginary parts of the complex eigenvalue

$$\int_0^H \frac{p_r}{p_r^2 + p_i^2} dx = \frac{2n-1}{2} \pi \quad (n = 1, 2, \dots, \infty) \quad (3.13a)$$

$$\int_0^H \frac{p_i}{p_r^2 + p_i^2} dx = 0 \quad (3.13b)$$

where  $p_r$  and  $p_i$  are the real and imaginary parts of  $p(\omega, x)$ , respectively, which are functions of  $\omega_r$ ,  $\omega_i$  and  $x$ .

In the case of undamped systems, the characteristic equation given by Equations (3.13) and the vibration mode given by Equation (3.10) become:

$$\omega_n \int_0^H \frac{1}{c(x)} dx = \frac{2n-1}{2} \pi \quad (n = 1, 2, \dots, \infty) \quad (3.14a)$$

$$\psi_n(z, \omega_n) = \lambda(z, \omega_n) \cos \left\{ \int_0^z \frac{\omega_n}{c(x)} dx \right\} \quad (3.14b)$$

where  $c(x) = \sqrt{\mu(x)/\rho(x)}$  is the shear wave velocity at depth  $x$ . This formula gives a rational basis for the following empirical relationship between the fundamental natural frequency of multi-layered systems,  $\bar{\omega}$ , and the material properties of the layers:

$$\bar{\omega} = \frac{\pi}{2} \left\{ \frac{H_1}{c_1} + \frac{H_2}{c_2} + \dots + \frac{H_N}{c_N} \right\}^{-1} \quad (3.15)$$

where  $c_j$  and  $H_j$  ( $J=1, 2, \dots, N$ ) are the shear wave velocity and the thickness of  $J$ th layer, respectively.

In the case of a multi-layered system, the continuity of displacement and stress between two adjacent layers should be considered. Let  $J$  be the suffix to express the values of each layer. The continuity between  $(J-1)$ th and  $J$ th layers requires the following relationships

$$\begin{Bmatrix} U_J(0) \\ \tau_J(0) \end{Bmatrix} = \begin{Bmatrix} U_{J-1}(H_{J-1}) \\ \tau_{J-1}(H_{J-1}) \end{Bmatrix}. \quad (3.16)$$

Substituting Equation (2.22) into Equation (3.16), the following result is obtained

$$\begin{Bmatrix} U_J(z_J) \\ \tau_J(z_J) \end{Bmatrix} = A_J(z_J) \cdot A_{J-1}(H_{J-1}) \cdot \dots \cdot A_1(H_1) \begin{Bmatrix} U_1(0) \\ 0 \end{Bmatrix}. \quad (3.17)$$

The eigenvalues  $\omega_n$  of layered system are given by the characteristic equation

$$U_N(H_N, \omega_n) = 0 \quad (n = 1, 2, \dots, \infty) \quad (3.18)$$

where  $N$  is the number of layers. The eigenfunction for each eigenvalue is given by

$$\psi_n(z_J, \omega_n) = U_J(z_J, \omega_n) \Big|_{U(0)=1} \quad \begin{cases} J = 1, 2, \dots, N \\ n = 1, 2, \dots, \infty \end{cases}. \quad (3.19)$$

### 3.3. Orthogonality of Undamped Vibration Mode Shapes

Proof of the orthogonality of the undamped vibration modes given by Equations (3.10) or (3.19) is not an easy task because of the implicit presence of multiple integrals in these equations. However, since the free vibration modes of a linear system obtained by using the multi-reflection theory possess orthogonality, the orthogonality of the undamped vibration modes given here is assured by the fact that the formulation of the non-linear harmonic wave solution is the result of application of the multi-reflection theory.

Let us return to Figure 2.1, which shows a soil layer subdivided into multiple layers of infinitesimal thickness. The equation of motion, Equation (2.2), is

$$\rho \frac{\partial^2 u}{\partial t^2} = \frac{\partial}{\partial z} \left( \mu \frac{\partial u}{\partial z} \right) + \frac{\partial}{\partial z} \left( \nu \frac{\partial^2 u}{\partial t \partial z} \right)$$

which is transformed into a set of linear equations for each sublayer, Equation (2.3), as

$$\rho_j \frac{\partial^2 u_j}{\partial t^2} = \mu_j \frac{\partial^2 u_j}{\partial z_j^2} + \nu_j \frac{\partial^3 u_j}{\partial t \partial z_j^2} \quad (j = 1, 2, \dots, m).$$

The second term on the right-hand side of the preceding equation should be zero when an undamped vibration mode is considered. It is assumed that the displacement in the layer can be expressed by the superposition of the undamped vibration modes,  $\Phi_n(z)$ , using normal coordinates  $S_n(t)$ ,

$$u(z, t) = \sum_n \Phi_n(z) S_n(t) \quad (3.20)$$

where

$$u(z) = \begin{cases} u_1(z_1) \\ u_2(z_2) \\ \vdots \\ u_m(z_m) \end{cases}, \Phi_n(z) = \begin{cases} \phi_1^n(z_1) & 0 \leq z \leq h_1 \\ \phi_2^n(z_2) & h_1 \leq z \leq h_2 \\ \vdots & \vdots \\ \phi_m^n(z_m) & h_{m-1} \leq z \leq h_m \end{cases} \quad (3.21)$$

in which  $u_j$ ,  $\phi_j^n$  ( $j=1,2,\dots,m$ ) are the displacement and the  $n$ th undamped vibration mode shape in the  $j$ th sub-layer, and  $\phi_j^n(z_j)$  is given by

$$\phi_j^n(z_j) = a_j \exp(p_j z_j) + b_j \exp(-p_j z_j), \quad p_j = \frac{\omega_n}{c_j} \quad (3.22)$$

$\omega_n$  is the  $n$ th natural circular frequency and  $c_j = \sqrt{\mu_j/\rho_j}$ . Substituting Equations (3.20), (3.21), (3.22) in Equation (2.2) and considering Equation (2.3), the equation of motion is rewritten

$$\sum_n \ddot{S}_n \Phi_n = \sum_n c^2 \Phi_n'' S + \sum_n \epsilon^2 \Phi_n'' \dot{S} \quad (3.23)$$

where

$$c(z) = \begin{cases} c_1 = \sqrt{\mu_1/\rho_1} \\ c_2 = \sqrt{\mu_2/\rho_2} \\ \vdots \\ c_m = \sqrt{\mu_m/\rho_m} \end{cases}, \epsilon(z) = \begin{cases} \epsilon_1 = \sqrt{\nu_1/\rho_1} & 0 \leq z \leq h_1 \\ \epsilon_2 = \sqrt{\nu_2/\rho_2} & h_1 \leq z \leq h_2 \\ \vdots & \vdots \\ \epsilon_m = \sqrt{\nu_m/\rho_m} & h_{m-1} \leq z \leq h_m \end{cases}$$

The second derivatives of mode shapes, which appear in Equation (3.23), have the following relationships if we consider Equation (3.22)

$$c^2 \Phi_n'' = -\omega_n^2 \Phi_n \quad \epsilon^2 \Phi_n'' = -\left(\frac{\epsilon}{c}\right)^2 \omega_n^2 \Phi_n \quad (3.24)$$

The orthogonality of  $\Phi_n$  is expressed as follows

$$\int_0^H \Phi_j(z) \Phi_n(z) dz = \alpha_j \delta_{jn} \quad (3.25)$$

where  $\delta_{jn}$  is the Kronecker delta. Substituting Equation (3.24) in Equation (3.23) and using the orthogonal relationship given by Equation (3.25), the following normal coordinate equation

is obtained which has a coupling term due to damping which arises because the vibration mode shapes in the damped system are not the same as the undamped mode shapes.

$$\alpha_n \ddot{S}_n + \sum_l \int_0^H \Phi_n(z) \left( \frac{\epsilon}{c} \right)^2 \omega_l^2 \Phi_l(z) dz \dot{S}_l + \alpha_n \omega_n^2 S_n = 0. \quad (3.26)$$

At the limit, the thickness of sub-layer goes to zero and  $\Phi_n(z)$  coincides with the undamped vibration mode shape  $\psi_n(z, \omega_n)$ .

### 3.4. The Dynamic Response of Soil Layer

The orthogonal properties of the normal coordinates was used in order to simplify the equations of motion in the layered system. When the base rock motion is given by  $u_g$ , the equation of motion expressed by Equation (2.2) is rewritten in terms of relative displacement as

$$\rho(z) \frac{\partial^2 u}{\partial t^2} + \rho(z) \ddot{u}_g = \frac{\partial}{\partial z} \left[ \mu \frac{\partial u}{\partial z} \right] + \frac{\partial}{\partial z} \left[ \nu \frac{\partial^2 u}{\partial t \partial z} \right]. \quad (3.27)$$

This equation can be written in terms of the normal coordinates,  $S_n(t)$ , as

$$\ddot{S}_n + 2 \sum_l h_{nl}^* \omega_l \dot{S}_l + \omega_n^2 S_n = -\ddot{f}_n \quad (3.28)$$

where

$$\ddot{f}_n = \frac{1}{\alpha_n} \int_0^H \psi_n(z, \omega_n) dz \ddot{u}_g, \quad \alpha_n = \int_0^H \psi_n^2(z, \omega_n) dz \quad (3.29)$$

$$2h_{nl}^* = \frac{\omega_l}{\alpha_n} \int_0^H \psi_n(z, \omega_n) \left[ \frac{\nu}{\mu} \right] \psi_l(z, \omega_l) dz. \quad (3.30)$$

If the soil properties of a layered medium do not show nonlinearity, the natural frequencies and mode shapes can be determined directly from Equation (3.18) and (3.19). However, if the non-linear behaviour of soil becomes predominant, the distribution of the shear strain magnitude along the depth will have to be given beforehand to determine  $\omega_n$  and  $\psi_n(z, \omega_n)$ , because the shear modulus and shear viscosity are functions of shear strain magnitude. Whatever shear strain measure is used, it is a function of mode shape, natural frequencies and general coordinates of all modes.

In Section 3.1, the equivalent damping factor and the equivalent shear modulus were given as functions of the strain amplitude. Direct application of these results to random response is impossible because of the difficulty in defining the shear strain amplitude during a random time history. However, if the probability density  $p(\gamma_0)$  of the peak amplitude  $\gamma_0$  in random response is determined, the equivalent linearization parameters for random response can be defined as their expectations using  $p(\gamma_0)$ . This procedure follows the suggestion of Liu [14] and the theoretical results obtained by Kobori and Minai [15]. Thus, in the case of stationary random response, the equivalent shear modulus and damping factor are defined as a function of the root-mean-square of strain,  $\sigma_\gamma$ , in the following form

$$\mu(\sigma_\gamma) = \int_0^\infty \mu(\gamma_0) p(\gamma_0, \sigma_\gamma) d\gamma_0 \quad (3.31a)$$

$$\zeta(\sigma_\gamma) = \int_0^\infty \zeta(\gamma_0) p(\gamma_0, \sigma_\gamma) d\gamma_0. \quad (3.31b)$$

Because of the nonproportional relation of the shear viscosity to shear modulus, the damping matrix  $h_{nl}^*$  appearing in Equation (3.28) is not a diagonal matrix. As an approximate solution, one may find an equivalent diagonal matrix such that the equations of motion are decoupled. The root-mean-square of the shear strain can then be obtained through modal superposition as

$$\sigma_\gamma = \left[ \sum_l \sum_n \frac{d\psi_l}{dz} \frac{d\psi_n}{dz} \lambda_{0,ln} \right]^{1/2} \quad (3.32)$$

where

$$\lambda_{0,ln} = \text{Re} \left[ \int_0^\infty G_F(\omega) H_l(\omega) H_n^*(\omega) d\omega \right]$$

where  $G_F(\omega)$  is the one-sided power spectral density of the input,  $H_n(\omega)$ , is the complex frequency transfer function of a single-degree-of-freedom oscillator

$$H_n(\omega) = \frac{1}{(\omega_n^2 - \omega^2) + 2ih_n\omega_n\omega} \quad (3.33)$$

where  $h_n$  is the diagonalized damping ratio and the asterisk denotes the complex conjugate. A method for obtaining  $h_n$  will be presented in the following section.

Using the relations given by Equations (3.31), (3.32) and (3.33), equivalent linear parameters  $\mu$  and  $\zeta$  can be determined. However, it is quite difficult to solve these relationships explicitly. Therefore, an iterative method on a digital computer is used to find the numerical result of Equations (3.31), (3.32) and (3.33).

If the shear strain response is assumed to be a stationary Gaussian process, the probability density function of  $\gamma_0$  will be given by [16].

$$p(\eta) = \frac{1}{\sqrt{2\pi}} \frac{1}{\sqrt{1-\alpha^2}} \exp\left\{\frac{-\eta^2}{2(1-\alpha^2)}\right\} + \frac{\alpha\eta}{2} \left\{1 + \operatorname{erf}\left[\frac{\alpha\eta}{\sqrt{2-2\alpha^2}}\right]\right\} \exp\left[-\frac{\eta^2}{2}\right] \quad (3.34)$$

where  $\eta = \frac{\gamma_0}{\sigma_\gamma}$ ,  $\alpha = \frac{\lambda_2^2}{\lambda_0 \lambda_4}$  and  $\lambda_m$  ( $m=0,2,4$ ) is the  $m$ th spectral moment of the shear strain response (see Section 3.6) and  $\operatorname{erf}(\cdot)$  is the error function.

### 3.5. Decoupling of Non-linear Damping

The equations of motion in terms of normal coordinates for a system with nonproportional damping have the following form as given by Equation (3.28)

$$\ddot{S}_n + 2 \sum_l h_{nl}^* \omega_l \dot{S}_l + \omega_n^2 S_n = -f_n, \quad n = 1, 2, \dots$$

The purpose of this section is to find an equivalent uncoupled modal damping ratio  $h_n$ . The uncoupled equation of motion in terms of  $h_n$  is

$$\ddot{S}_n + 2 h_n \omega_n \dot{S}_n + \omega_n^2 S_n = -f_n. \quad (3.35)$$

The expectation of the mean square error due to the decoupling term can be written as

$$E[e^2] = E\left[2 \sum_l h_{nl}^* \omega_l \dot{S}_l - 2 h_n \omega_n \dot{S}_n\right]^2. \quad (3.36)$$

Minimizing  $E[e^2]$  with respect to  $h_n$ :  $\partial E[e^2]/\partial h_n = 0$ , we obtain the equivalent decoupled damping ratio  $h_n$  as a function of the normal coordinate

$$h_n = \frac{\sum_l h_{nl}^* \omega_n \omega_l E[\dot{S}_n \dot{S}_l]}{\omega_n^2 E[\dot{S}_n^2]}. \quad (3.37)$$

The values of the denominator and numerator are expressed in terms of the second cross-spectral moment

$$E[\dot{S}_n \dot{S}_l] = \lambda_{2,nl} . \quad (3.38)$$

Substituting Equation (3.38) for Equation (3.37), the equivalent decoupled damping ratio associated with the least mean-square error is obtained as follows

$$h_n = \frac{\sum_l h_{nl}^* \lambda_{2,nl} \omega_l}{\lambda_{2,nn} \omega_n} . \quad (3.39)$$

It is noted that the cross-spectral moments in the numerator are only significant when modes are closely spaced.

This same result can be obtained by equating the expected energy dissipation of the two systems, i.e.

$$2 h_n \omega_n E[\dot{S}_n^2] = 2 \sum_l h_{nl} \omega_l E[\dot{S}_n \dot{S}_l] . \quad (3.40)$$

It is interesting to note that the two different criteria for decoupling of normal coordinates result in the same expression for expressing the decoupled damping ratio.

### 3.6. Determination of Soil Response Based on Response Spectrum

If the input motion  $u_g$  is given deterministically, a seismic response analysis based on any numerical integration technique can be carried out resulting in the time history of the response quantity of interest. However, the soil layer response quantities are generally strongly affected by the choice of the input time history. Thus, the use of a single input time history, even if it is defined with due consideration to the potential earthquake magnitude, epicentral distance, and the condition of geological topography, leaves considerable uncertainty in the seismic analysis.

One way to overcome this problem is to use an average response measure which includes the statistical nature of the earthquake motion. The response spectrum method for stationary random vibration analysis proposed by Der Kiureghian [12] is appropriate for this purpose. A brief summary of his results follows.

For each normal coordinate, three spectral moments  $\lambda_{m,nn}$  ( $m=0,1,2$ ) are given in terms of the mean-response spectrum,  $\bar{S}_T(\omega_n, h_n)$ , which is the mean of the absolute maximum of the

$n$ th normal coordinate  $S_n(t)$  over duration  $T$ :

$$\lambda_{0,nn} = \frac{1}{p_n^2} \bar{S}_T^2(\omega_n, h_n) \quad (3.41a)$$

$$\lambda_{1,nn} = \frac{\omega_n \sqrt{1-4h_n/\pi}}{p_n^2} \bar{S}_T^2(\omega_n, h_n) \quad (3.41b)$$

$$\lambda_{2,nn} = \frac{\omega_n^2}{p_n^2} \bar{S}_T^2(\omega_n, h_n) \quad (3.41c)$$

where  $p_n$  is a peak factor given as a function of the natural frequency  $\omega_n$  and the damping ratio  $h_n$  of the  $n$ th mode [12]. This allows computation of the spectral moments of the response from the superposition relation

$$\lambda_m = \sum_n \sum_l \Psi_n \Psi_l \rho_{m,nl} \sqrt{\lambda_{m,nn} \lambda_{m,ll}}, \quad m = 0,1,2 \quad (3.42)$$

where  $\Psi_n$  is the effective participation factor of the  $n$ th mode (for the deformation  $\Psi_n = \alpha_n \psi_n(z)$  and for the shear strain  $\Psi_n = \alpha_n \partial \psi_n(z) / \partial z$ ), and  $\rho_{m,nl}$  are correlation coefficients which are given in terms of natural frequencies  $\omega_n$  and  $\omega_l$  and damping ratios  $h_n$  and  $h_l$  [12].  $p$  and  $q$  in the last two equations are peak factors which are given as functions of the spectral moments  $\lambda_m$  ( $m=0,1,2$ ) of the response. Based on these equations, modal combination rules are developed for various statistical response quantities such as the root-mean-square  $\sigma_R$ , the root-mean-square of response rate  $\sigma_{\dot{R}}$ , the mean of the peak response  $\bar{R}_T$  and the standard deviation of the peak response  $\sigma_{R_T}$  over duration  $T$ . These quantities are given in terms of the response spectrum as follows:

$$\sigma_R = \left[ \sum_n \sum_l \frac{1}{p_n p_l} \rho_{0,nl} \Psi_n \Psi_l \bar{S}_T(\omega_n, h_n) \bar{S}_T(\omega_l, h_l) \right]^{1/2} \quad (3.43a)$$

$$\sigma_{\dot{R}} = \left[ \sum_n \sum_l \frac{\omega_n \omega_l}{p_n p_l} \rho_{2,nl} \Psi_n \Psi_l \bar{S}_T(\omega_n, h_n) \bar{S}_T(\omega_l, h_l) \right]^{1/2} \quad (3.43b)$$

$$\bar{R}_T = p \sigma_R \quad (3.43c)$$

$$\sigma_{R_T} = q \sigma_R \quad (3.43d)$$

Another quantity that is used for evaluating the equivalent viscous damping factor given in Equation (3.2) is the response mean frequency denoted by  $\bar{\omega} = \sigma_{\dot{R}} / \sigma_R$ . Substituting  $\bar{\omega}$  into Equation (3.2), the ratio of  $\nu$  to  $\mu$  is expressed by

$$\frac{\nu}{\mu} = 2 \frac{\xi}{\bar{\omega}} . \quad (3.44)$$

This estimation of  $\nu/\mu$  can be used for the evaluation of nonproportional damping given by Equation (3.30).

### 3.7. Application

The material properties of ground used in the numerical example are assumed as shown in Figure 3.2. The soil is assumed to be a two-layer system. The first layer is to represent the alluvium deposits and the second layer is to represent the diluvium deposits. The distribution of the non-linear parameter of soil,  $\alpha$ , given by Equation (3.5) and the shear wave velocity at infinitesimal strain level,  $c_s$ , are illustrated in Figure 3.2. These values are calculated from Equations (3.5) and (3.7), using  $c'=0.01\text{kg/cm}^2$ ,  $\phi'=35^\circ$ ,  $K_0=0.5$ ,  $D=60.7$  and  $a=0.9$ . The average values of shear wave velocities of the two layers are 160m/sec and 320m/sec, respectively. These values are used as the material properties of homogeneous layers for comparison with the results for the inhomogeneous layers.

In order to examine the influence of the number of terms in the series expansion of  $\kappa$ 's power on the accuracy of results, some numerical computations are performed for inhomogeneous layers without consideration of the non-linear properties of the soil. The results are shown in Figure 3.3. The first three mode shapes are shown in this figure computed based on the first to the fifth order of  $\kappa$ 's power. It can be seen from this figure that the order of  $\kappa$ 's power has little influence on the modal shapes. Even the first order gives quite good results. Because of the simple formula of the first term, which is given by Equation (3.14b), this result can be used to reduce the computational effort. In addition, closed form analytical expressions of modal shapes can be obtained for certain types of inhomogeneous distributions of soil properties, provided the integration of the inverse of the shear wave velocity distribution function exists in closed form. In Figure 3.4(a), the calculated results based on the multi-reflection theory are shown. Each layer is subdivided into twenty sub-layers. The modal shapes completely coincide with those in Figure 3.3 obtained by the proposed method if the  $\kappa$ 's power is greater than three.

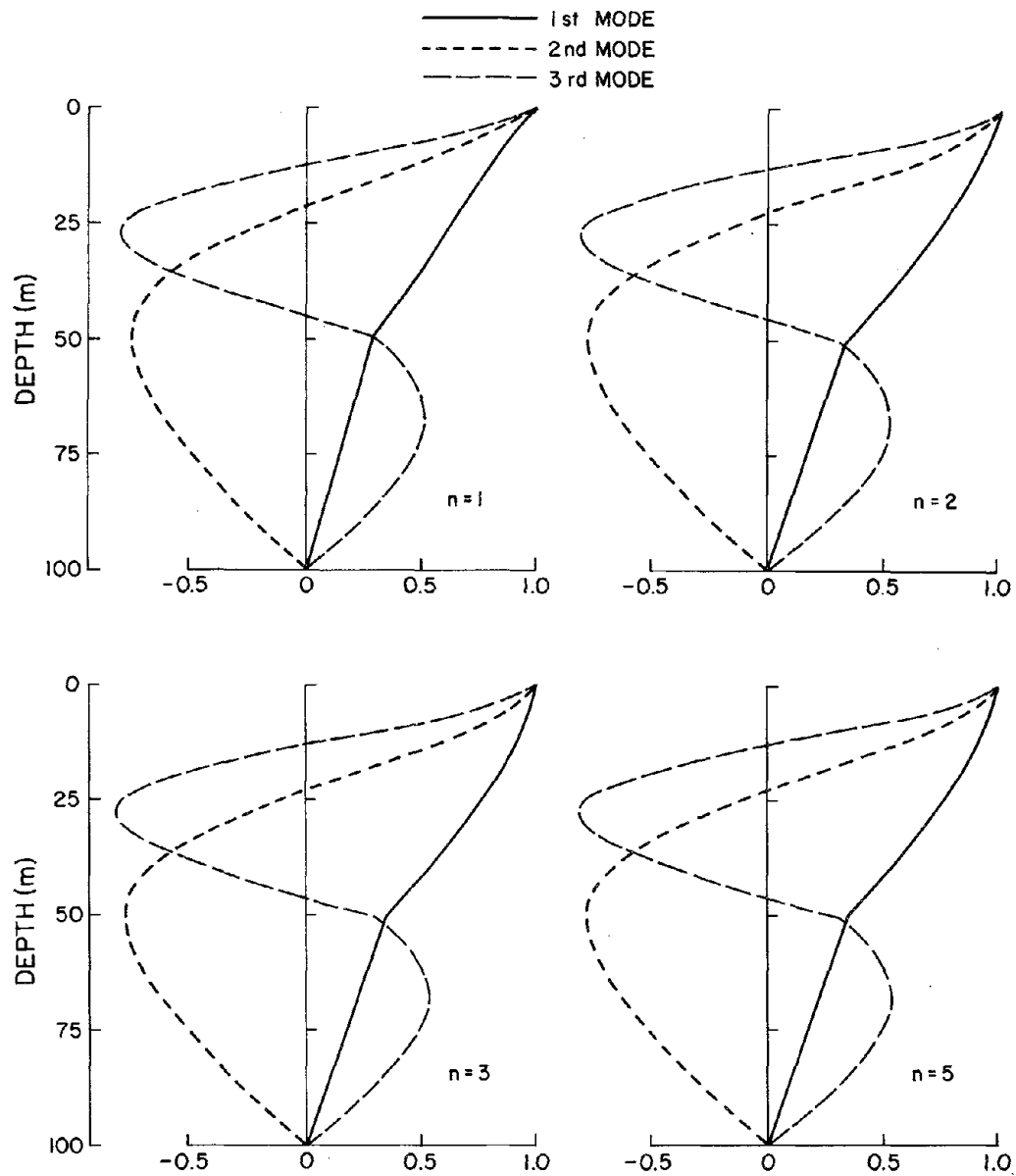
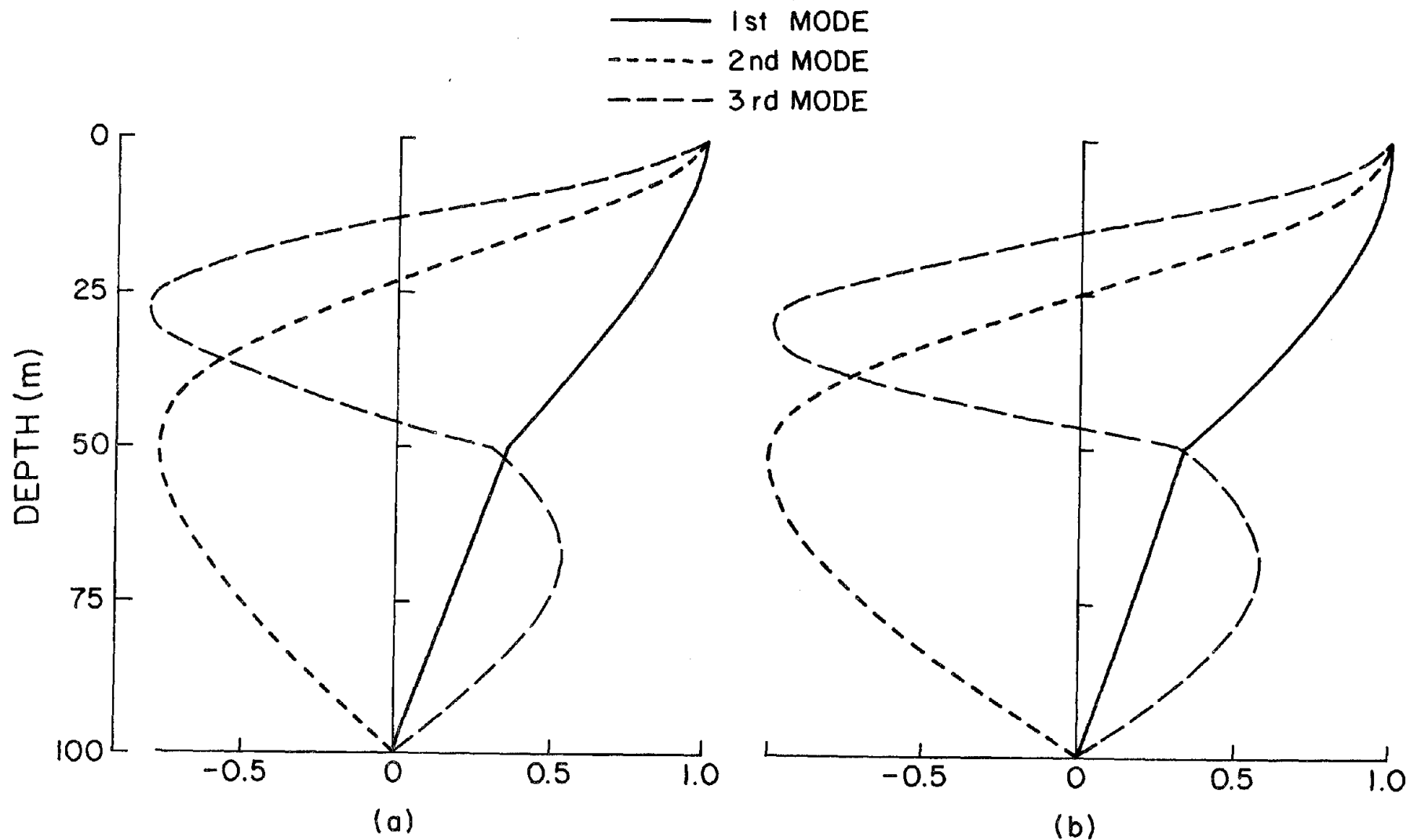


Figure 3.3 Mode shapes for example case showing influence of  $\kappa$  terms



**Figure 3.4** Mode shapes for: (a) inhomogeneous layers based on multi-reflection theory; (b) homogeneous layers

In the case where the soil layers have homogeneous characteristics, see Figure 3.4(b), although the modal shapes are somewhat different for higher modes, their overall shapes are very similar to those of the inhomogeneous soil layers in Figure 3.4(a).

Table 3.1 shows a comparison of natural frequencies. Included in this table are natural frequencies for the first five modes computed considering various powers of  $\kappa$  and the exact solutions based on the multi-reflection theory. Natural frequencies for the homogeneous layered system are also included in the last column of the table. It can be observed in this table that natural frequencies obtained from the characteristic equation based on powers of  $\kappa$  greater than two are in close agreement with the exact solutions. The simplified case of the first order of  $\kappa$ 's power, in which none of  $\kappa$ 's terms appear in the characteristic equation, also yields good results especially for the higher modes. Note that the assumption of homogeneous layered system is adequate for a rough estimate of the natural frequencies of inhomogeneous layers if material properties of homogeneous layers are assumed to coincide with average material properties of the corresponding inhomogeneous layers.

To calculate the mean of the peak ground response based on the above mentioned procedure, the mean response spectrum should be prescribed. There have been many proposals for developing response spectra for practical design purposes. Recent researches have developed attenuation laws for spectral amplitudes expressed in terms of the earthquake magnitude,  $M$ , source-to-site distance,  $\Delta$ , and the type of geological environment surrounding the site [17,18]. In this analysis, McGuire's relationships [17] are used. The relationship between the pseudo-velocity response spectrum  $S$  and the above mentioned earthquake parameters is given by

$$S(\omega) = a(\omega)10^{b(\omega)M}(\Delta + 25)^{-c(\omega)} \quad (3.45)$$

where  $a(\omega)$ ,  $b(\omega)$  and  $c(\omega)$  are given based on regression analyses as functions of the natural frequency of a single-degree-of-freedom system  $\omega$ . This relationship is obtained for the damping ratio of 2%. The modification of this relationship for other damping ratio is done by multiplying by the factor given in Figure 3.5. In the following analyses,  $\Delta=40\text{km}$  and  $M=7$  are used

TABLE 3.1  
 NATURAL FREQUENCIES FOR FIRST FIFTH MODES

		Order of $\kappa$ 's Power				Multi-Reflection Theory	Homogeneous Case
		1	2	3	5		
Natural Frequency for Each Mode Hz	1	0.582	0.649	0.656	0.657	0.658	0.627
	2	1.575	1.614	1.619	1.619	1.621	1.600
	3	2.558	2.580	2.584	2.584	2.588	2.573
	4	3.721	3.734	3.736	3.736	3.741	3.827
	5	4.726	4.734	4.735	4.735	4.741	4.800

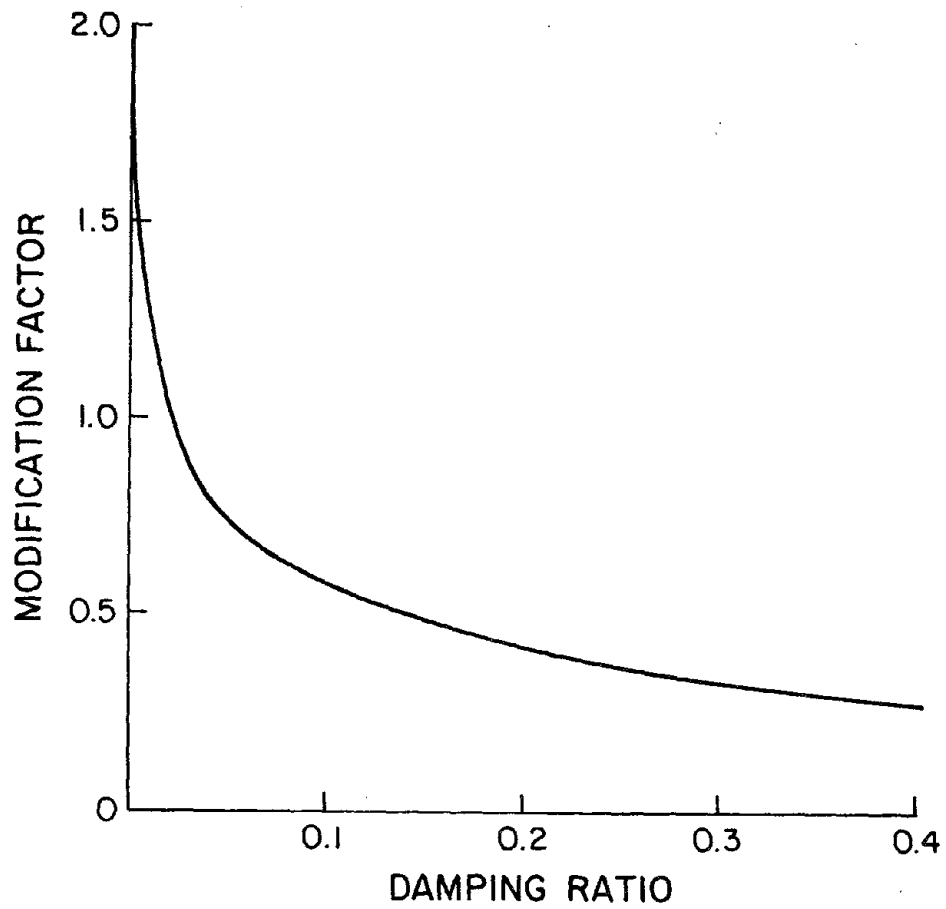


Figure 3.5 Factor for modifying Equation 3.45 for various damping values

except when otherwise specified.

The modal damping ratio is one of the most important factors in estimating the response quantities. The damping nature of soil is frequency independent and mainly consists of hysteretic damping. Therefore, the modal damping ratio cannot be given directly without first giving consideration to the non-linear response of the soil element. This point will be further discussed in the next paragraph. Here we use 20% damping ratio for each mode. Figures 3.6(a) and 3.6(b) show the estimated mean peak response for velocity and shear stress distribution based on Equation (3.43c). It is clear from these figures that the  $\kappa$ 's terms hardly affect the response quantities. Another factor which should be considered in using the modal analysis is the number of superposing modes. Figures 3.7(a) and 3.7(b) show the effect of the number of superposing modes on the response quantities. The result obtained by superposing more than three modes is acceptable for practical purposes. Figure 3.8(a) and 3.8(b) are comparisons of response quantities of the homogeneous and inhomogeneous systems. It is observed that if the inhomogeneity of the soil layer is not too strong, it is reasonable to assume that the actual layered ground is homogeneous.

The effect of the modal damping ratio on response quantities are examined in Figures 3.9(a) and 3.9(b). The same damping ratio for each mode is assigned and changed from 5 to 40%. The response magnitude is strongly affected by damping ratios; for example the velocity response at ground surface for 5% damping ratio is four times greater than that for 40% damping ratio. These results suggest that the modal damping must be determined more rigorously. One way to solve this problem is to use the method proposed in Section 3; i.e., non-linear response analysis based on the equivalent linearization technique. The distribution of the equivalent material damping factor with depth can be calculated from Equation (3.4) and the ratio  $\nu/\mu$  is given by Equation (3.2), so that the coupled modal damping matrix is obtained using Equation (3.30). The equivalent decoupled modal damping ratio associated with the least mean-square error is obtained using Equation (3.39).

The decrease in the shear wave velocity due to the nonlinear behavior of soil is shown in

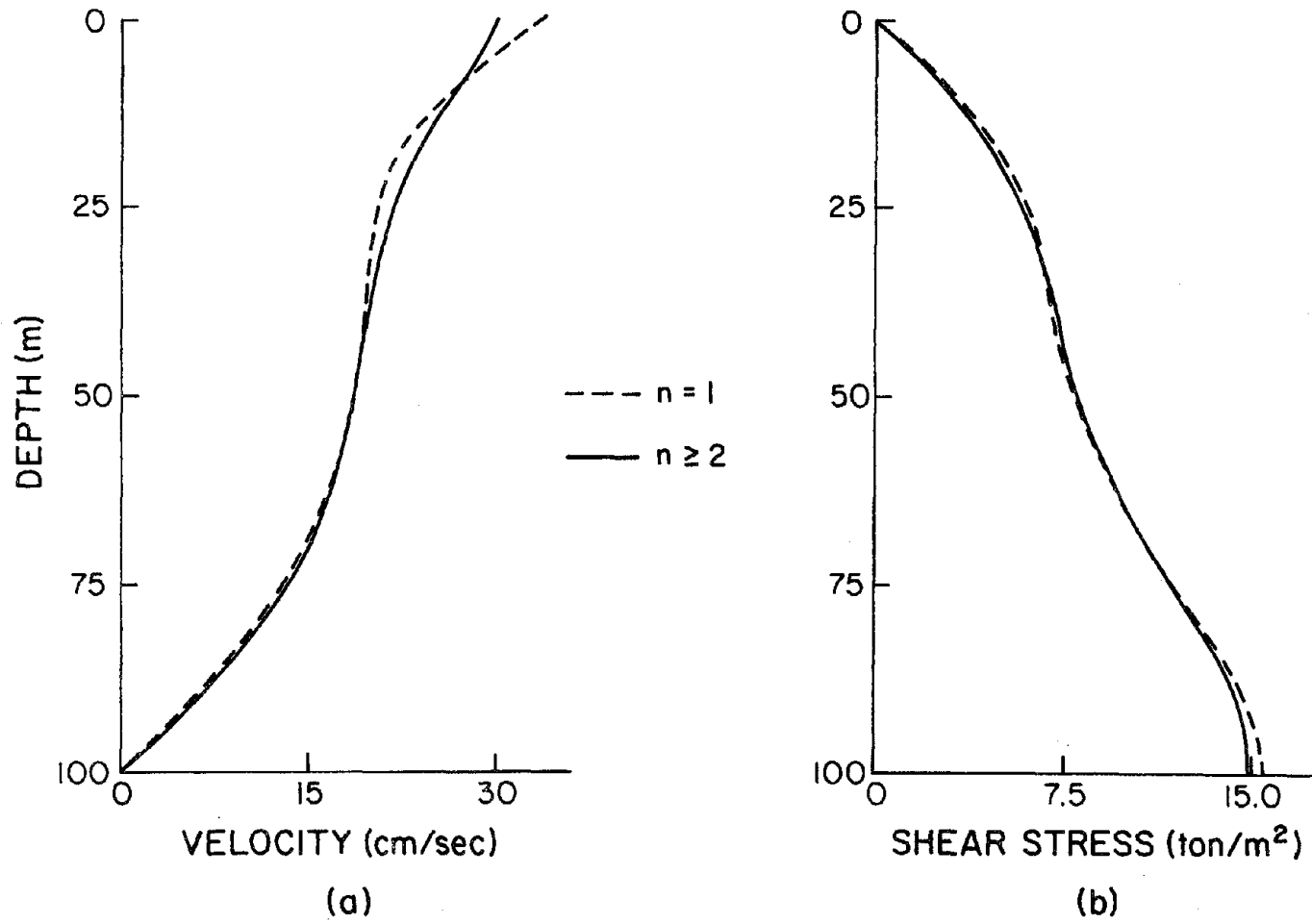


Figure 3.6 Estimated mean peak responses showing effect of  $\kappa$  terms;  $\Delta=40\text{km}$ ,  $M=7$

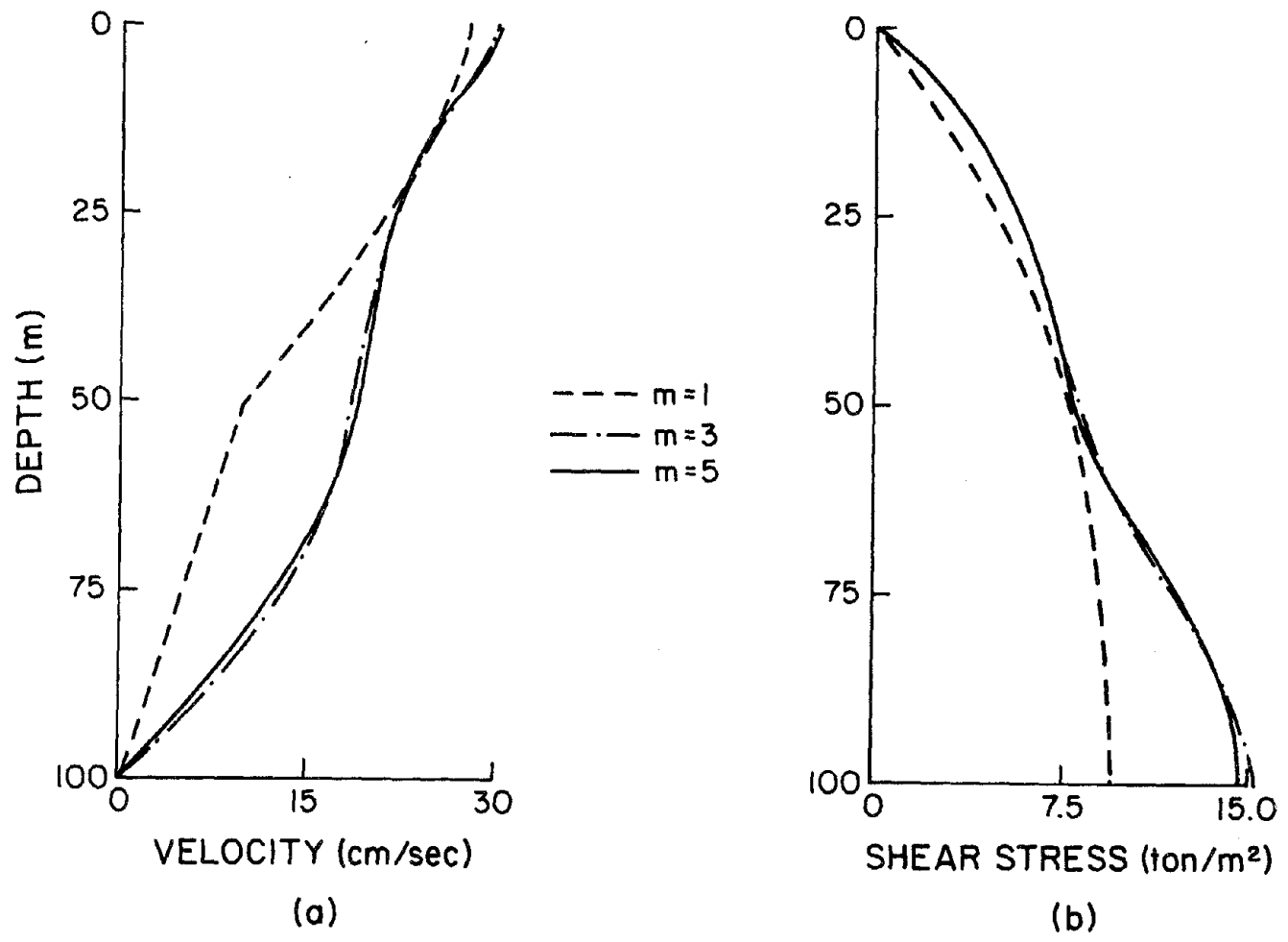
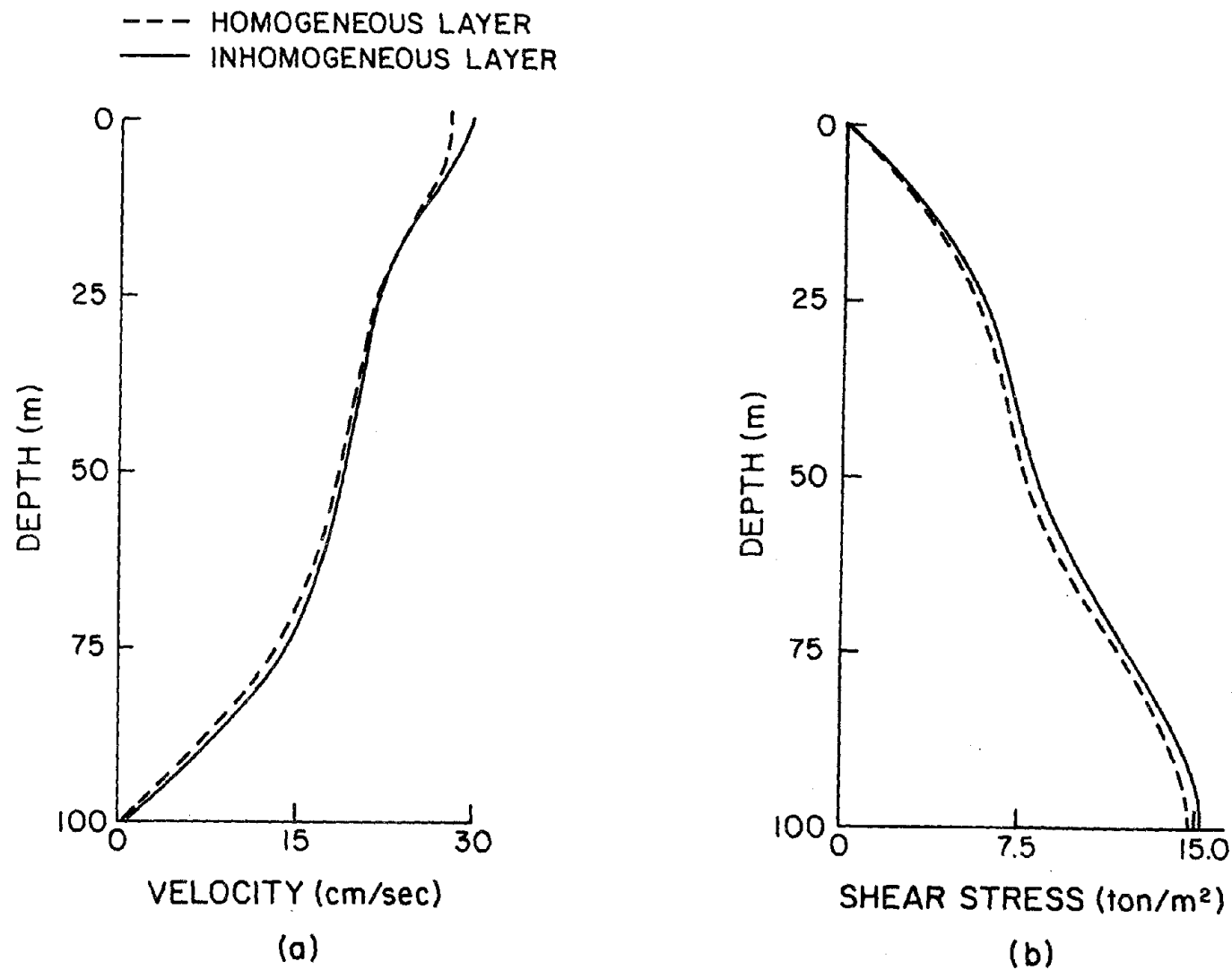
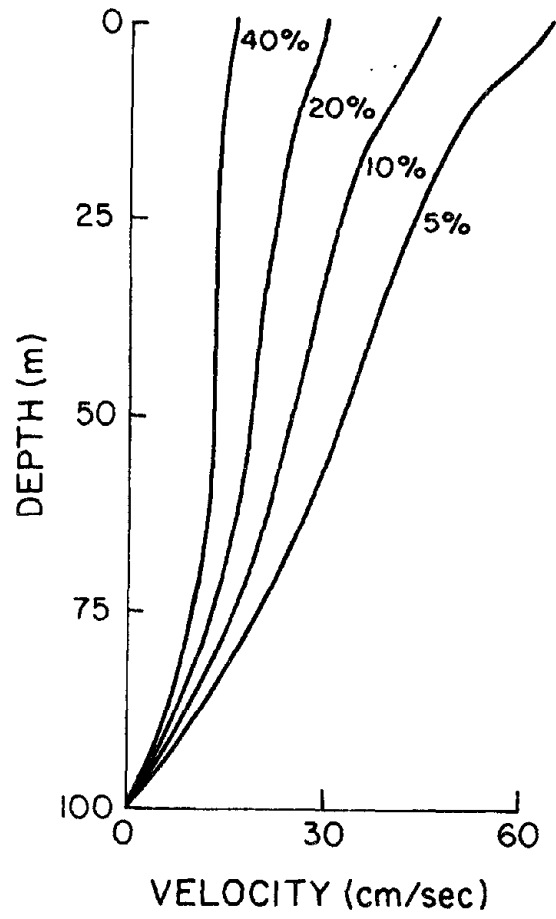


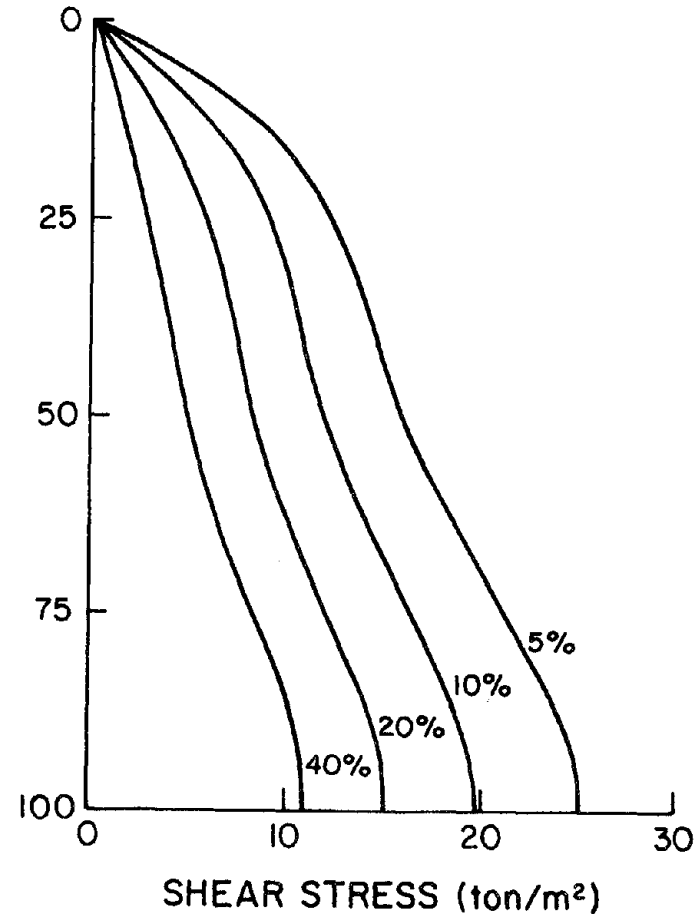
Figure 3.7 Estimated mean peak responses for various numbers of superposing modes;  $\Delta=40$  km,  $M=7$



**Figure 3.8** Estimated mean peak responses showing effect of soil inhomogeneity;  $\Delta=40\text{km}$ ,  $M=7$



(a)



(b)

Figure 3.9 Estimated mean peak responses showing effect of damping;  $\Delta=40\text{km}$ ,  $M=7$

Figure 3.10 as a percentage of the initial value. Figure 3.11 shows the distribution of the equivalent material damping with depth. The results are shown for epicentral distances of 40 and 160km. From these figures, it is observed that there is a large decrease in the shear wave velocity near ground surface and that the damping factor near ground surface is very high. In these calculations,  $\epsilon$  the ratio between the expectation of the zero crossing rate and the total number of peaks per unit time, is taken to be 0.8.

Figure 3.12 is the relation between the epicentral distance and the damping ratio for each mode. The damping ratios for modes higher than the third mode are very high and in the case of the fourth mode, overdamping is indicated. Note that the damping ratio is relatively insensitive to the epicentral distance for the first two modes. This result suggests using a constant strain independent modal damping ratio for all epicentral distances. At the epicentral distance of 40km, there are five circles shown in Figure 3.12 which correspond to the decoupled modal damping ratios obtained by ignoring the off-diagonal terms in a coupled modal damping matrix. The numbers indicate the corresponding modes. It is observed that this method gives a low estimate of the modal damping for higher frequency modes. This implies that the contributions from higher modes are overestimated in this approach.

Figure 3.13(a) shows shear stress distributions for different epicentral distances. The results are obtained by considering initial inhomogeneity and non-linearity of the soil layer. In the case of  $\Delta=40$ km, the stress distribution is also shown for the layers which initially possessed homogeneous nature. Comparing these results with those given in Figure 3.8(b), it is obvious that the stress distribution is hardly affected by the inhomogeneity and non-linearity of the soil layer. This means that a sophisticated analysis which considers both the inhomogeneity and non-linearity of soil properties is not necessary from a practical point of view and that the linear analysis of homogeneous layer gives adequate information for stress distributions. To investigate the dependency of the stress distribution on the epicentral distance, the stress distributions given in Figure 3.3(a) are normalized by using the mean of the peak velocity at ground surface. The normalized results, Figure 3.3(b), show that the shape of stress distribution is

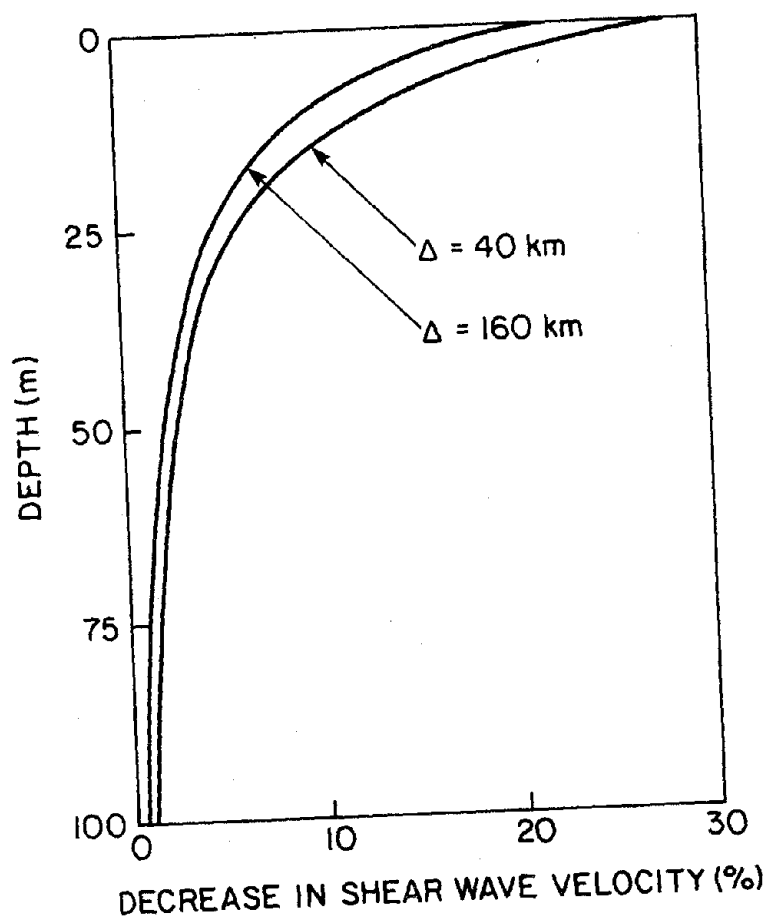


Figure 3.10 Decrease in shear wave velocity as percentage of initial value;  $M=7$

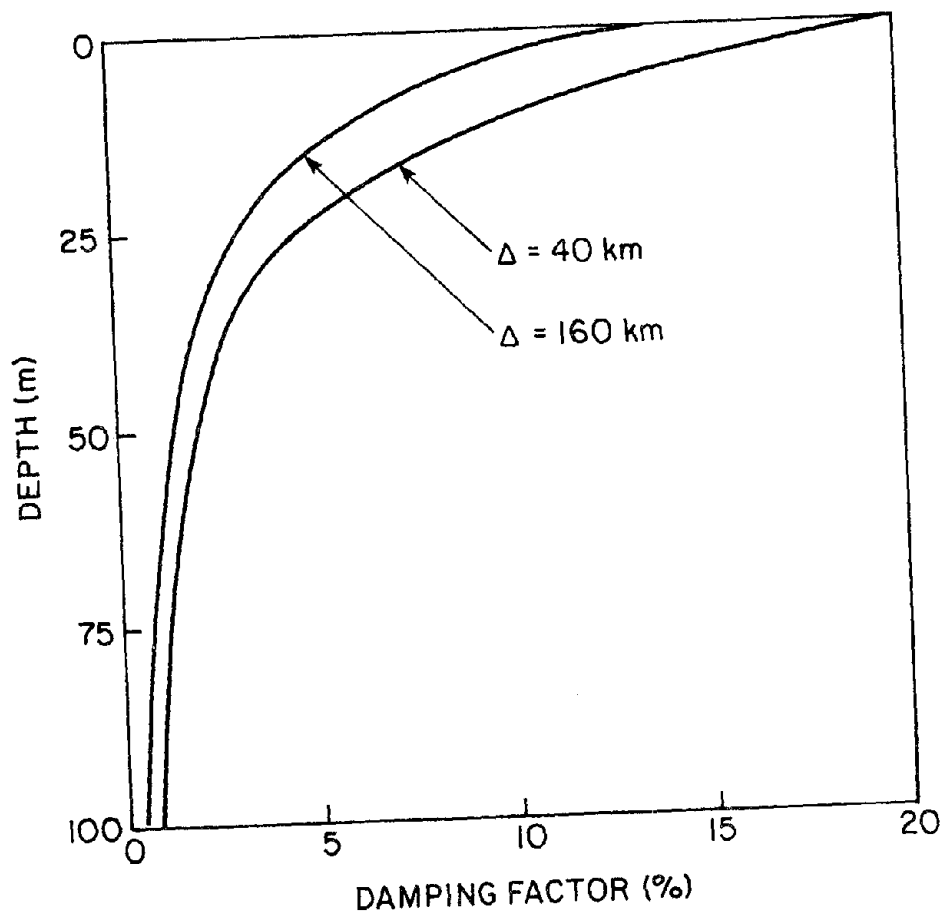
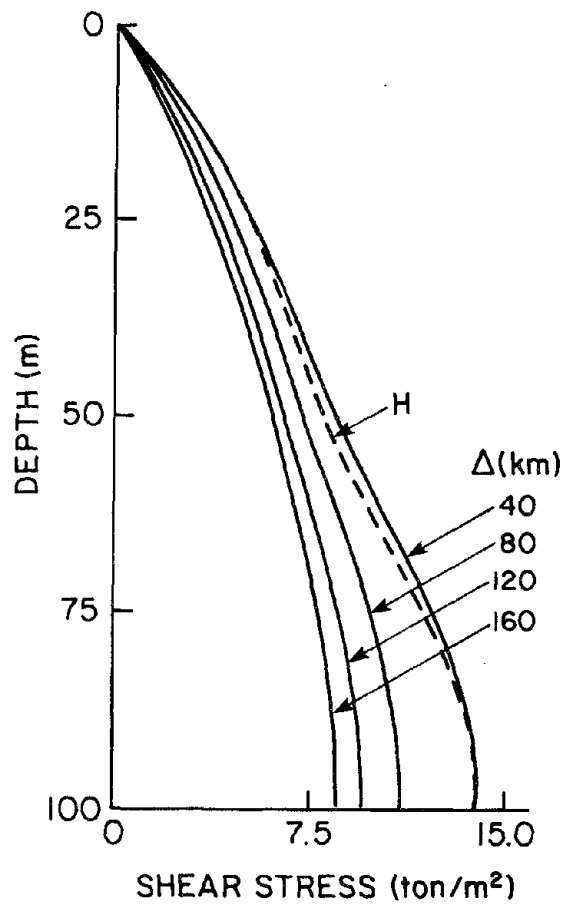
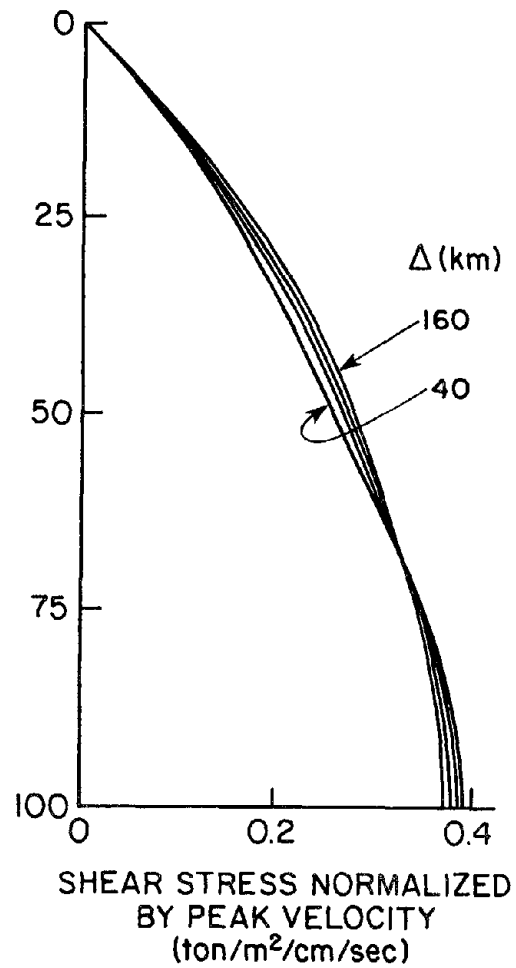


Figure 3.11 Distribution of equivalent material damping with depth;  $M=7$



(a)



(b)

**Figure 3.13 Distributions of mean peak shear stress for various epicentral distances;  $M=7$**

practically independent of the epicentral distance.

The stress distribution is one of the most tolerant measures of response because it is not strongly affected by the local geological conditions. However, other response quantities such as the shear strain show stronger dependency on the local geology as shown in Figure 3.14.

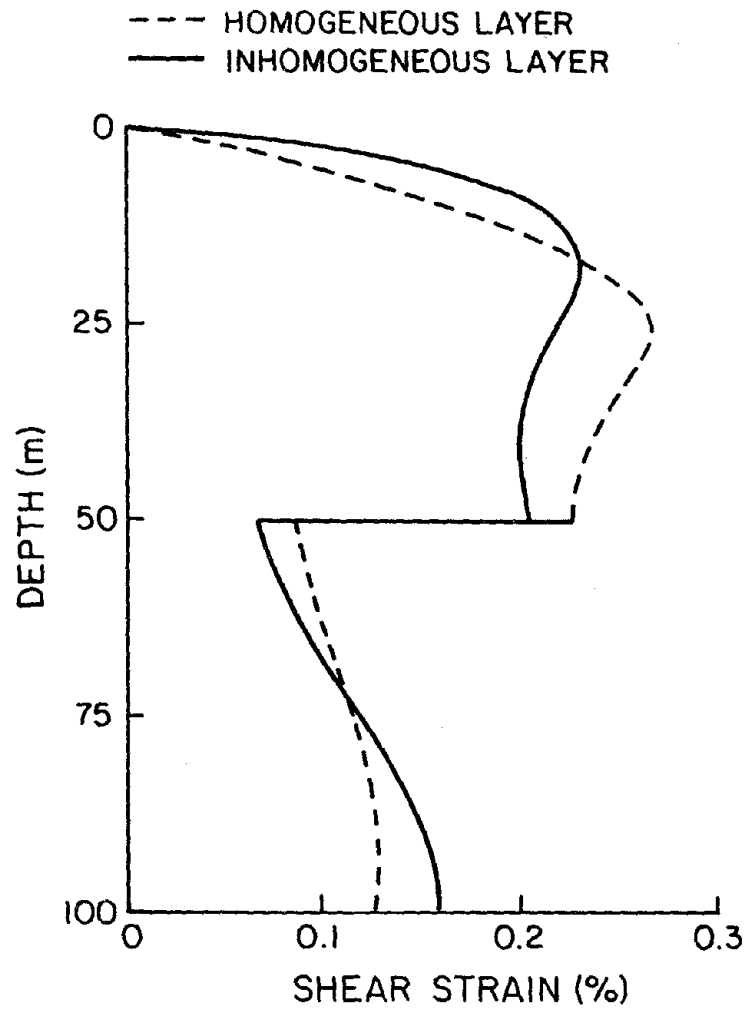


Figure 3.14 Estimated mean peak shear strain showing effect of soil inhomogeneity;  $\Delta=40\text{km}$ ,  $M=7$

#### 4. ANALYSES OF LIQUEFACTION PHENOMENA

It has recently become possible to obtain undisturbed sand samples and the liquefaction potential of actual ground sites can now be estimated based on the dynamic shear tests of undisturbed samples. However, it is important to note that this liquefaction potential is obtained from the dynamic triaxial or simple shear test results. Therefore, there are still many problems to be solved to clarify the relationship between the dynamic behaviour of ground and liquefaction during strong earthquakes. For the purpose of seismic risk analysis, for example, it is necessary to determine the relationship that exists between the earthquake magnitude, epicentral distance, and site condition and the liquefaction potential. The stress distribution with depth during strong earthquake motions was given in the preceding sections taking into consideration the stochastic nature of earthquake motions and resulting from the attenuation law of response spectra and site conditions. This result is used for calculating the liquefaction potential. Using the existing techniques for analyzing structural fatigue, the analytical bases for evaluating the fatigue life of loose sand layer against strong earthquakes is formulated.

##### 4.1. S-N Curve for Undrained Saturated Sand

Several methods such as cyclic triaxial, cyclic simple shear and torsional shear tests have been applied to simulate earthquake stress conditions on a particular soil element. The results obtained from cyclic simple shear tests by Peacock and Seed [19] are rearranged in Figure 4.1. This  $S-N$  curve can be expressed by the following equation

$$\frac{\tau}{p_v'} \frac{1}{D_r} = \frac{\alpha}{N^\beta} \quad (4.1)$$

where  $\tau$  is the cyclic shear stress amplitude applied to the potential failure surface,  $p_v'$  is the vertically effective stress applied to the potential failure surface before cyclic loading,  $D_r$  is the relative density of sand,  $N$  is the number of applied stress cycles required to cause failure, and  $\alpha$  and  $\beta$  are experimental constants.

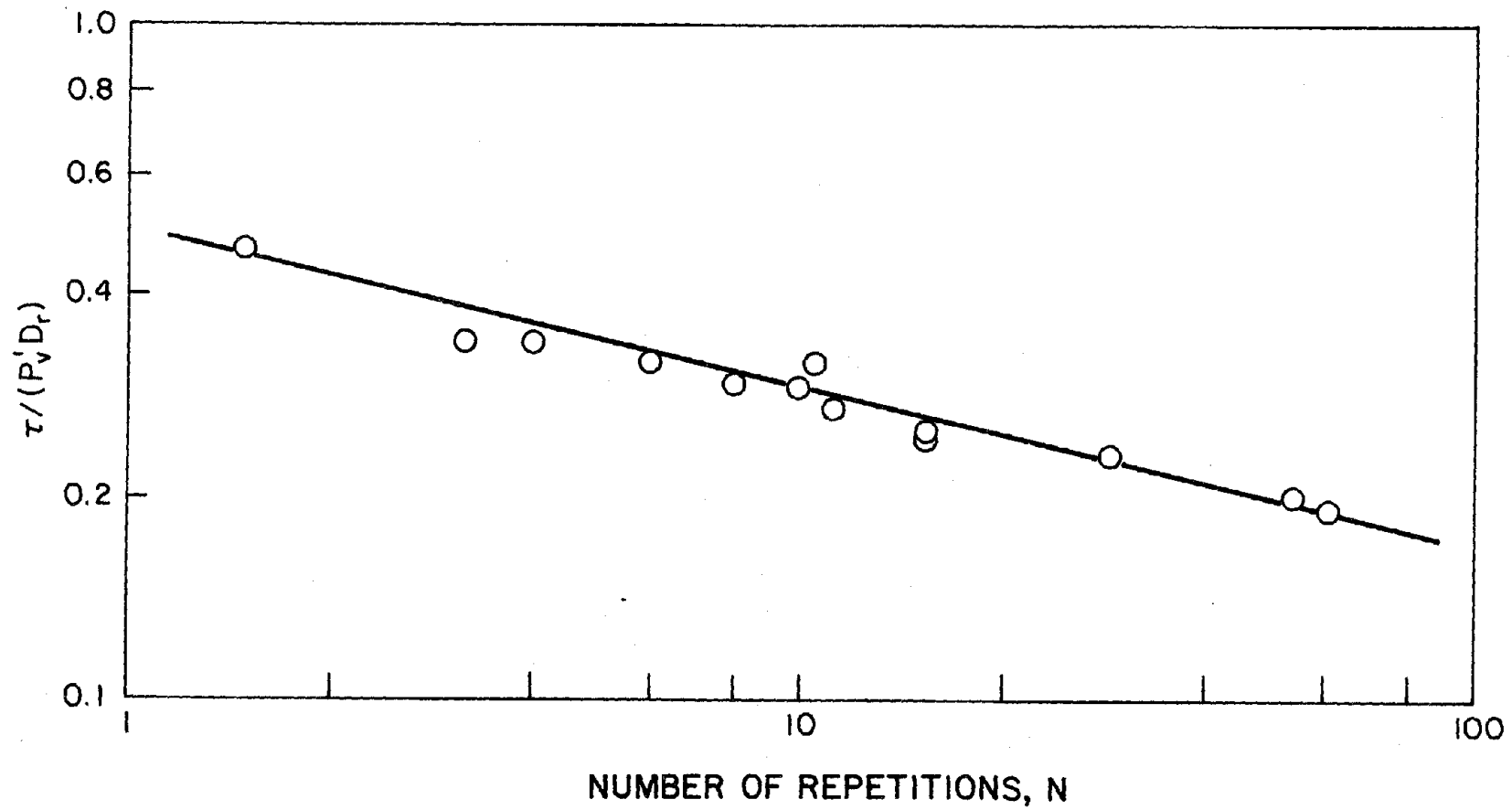


Figure 4.1 S-N curve based on test data by Peacock and Seed [19]

## 4.2. Fatigue Theory

Failure by fatigue is the result of cumulative damage caused by the repeated application of alternate loading and unloading cycles. The fatigue life of a material can be approximately determined on the basis of the  $S-N$  relationship and Miner's linear cumulative damage criterion. If the material is loaded  $n_i$  times with constant stress amplitude  $\tau_i$  with which  $N_i$  times loading causes failure of the material, the cumulative damage  $D$  can be expressed in the discrete form

$$D = \sum_i \frac{n_i}{N_i} \quad (4.2)$$

By substituting Equation (4.1) into Equation (4.2)

$$D = \sum_i n_i \left\{ \frac{\tau_i}{\alpha p_v D_r} \right\}^{\frac{1}{\beta}} \quad (4.3)$$

To apply the Miner's criterion to random loading cycles, the definition of  $n_i$  should be expanded so that it has a meaning for random loading conditions because the number of amplitude repetitions in a stochastic process are generally unknown. One applicable interpretation is that  $n_i$  expresses the number of peaks at a certain stress level  $\tau$ . In that case, the expectation of the cumulative damage per unit time,  $D(t)$ , can be written in the continuous form

$$E[D(t)] = \left\{ \frac{1}{\alpha p_v D_r} \right\}^{\frac{1}{\beta}} E[m] \int_0^{\infty} \tau^{\frac{1}{\beta}} p(\tau, t) d\tau \quad (4.4)$$

where  $E[m]$  is the expectation of the total number of peaks per unit time and  $p(\tau, t)$  is the distribution of the peaks of the shear stress response. If the random process is stationary,  $E[D(t)]$  reduces to a constant. Therefore, for stationary shear stress response, the expected total accumulated damage during duration  $T$  is given by

$$E[D_T] = T \cdot E[D] = T \cdot E[m] \left\{ \frac{1}{\alpha p_v D_r} \right\}^{\frac{1}{\beta}} \int_0^{\infty} \tau^{\frac{1}{\beta}} p(\tau) d\tau \quad (4.5)$$

If the  $S-N$  curve has a threshold level  $\tau_0$ , the integral region in Equation (4.5) should be above the threshold level, then

$$E[D_T] = T \cdot E[m] \left\{ \frac{1}{\alpha p_v D_r} \right\}^{\frac{1}{\beta}} \int_{\tau_0}^{\infty} (\tau - \tau_0)^{\frac{1}{\beta}} p(\tau) d\tau . \quad (4.6)$$

If the shear stress response is assumed to be a stationary Gaussian process, the peak distribution function of  $\tau$  is then given by Equation (3.34). Using  $\xi$  for  $\tau/\sigma_\tau$ , Equation (4.5) is rewritten as follows

$$E[D_T] = T \epsilon^{-1} f(\beta) \frac{\sigma_{\dot{\tau}}}{\sigma_\tau} \left\{ \frac{\sigma_\tau}{\alpha p_v D_r} \right\}^{\frac{1}{\beta}} , \quad f(\beta) = \int_0^{\infty} \xi^{\frac{1}{\beta}} p(\xi) d\xi . \quad (4.7)$$

In the special case when the response is assumed to be the output from a narrowband filter,  $p(\tau)$  is of Rayleigh form with  $\epsilon=1$ . The expectation of the total damage then becomes [20]

$$E[D_T] = \sqrt{2} \cdot T \cdot \Gamma \left\{ \frac{1 + 2\beta}{2\beta} \right\} \left\{ \frac{\sigma_\tau}{\alpha p_v D_r} \right\}^{\frac{1}{\beta}} \frac{\sigma_{\dot{\tau}}}{\sigma_\tau} \quad (4.8)$$

where  $\Gamma(\cdot)$  is the Gamma function,  $\sigma_\tau$  and  $\sigma_{\dot{\tau}}$  are the root-mean-squares of the stress response and the stress response rate, respectively.

The expected life left after random loading is obtained from the following equation

$$L_f = 1.0 - E[D_T] \quad (4.9)$$

when  $L_f$  reaches zero, the fatigue failure is assumed to occur.

### 4.3. Application

Using the  $S-N$  curve as given in Figure 4.1, the cumulative damage of liquefaction is calculated from Equation (4.7). Parameters  $\alpha$  and  $\beta$  are given by experiment to be  $\alpha=0.5$  and  $\beta=0.233$ . If  $\epsilon$  is given, the remaining factors which affect the liquefaction potential are the root-mean-squares of the stress and the stress rate, the effective vertical stress and the relative density. The damage caused by liquefaction process is directly proportional to the root-mean-square of the stress rate but proportional to the  $(1/\beta - 1)$ th power of root-mean-square of the stress. Based on the experimental data  $\beta=0.233$ , then  $(1/\beta - 1)=3.3$ . This means that the accuracy of stress estimation must be three times more than that of the stress rate. The accuracy of estimating the effective vertical pressure and the relative density is more significant

compared with the accuracy of the stress estimation because the influence factor of error propagation is about  $4(=1/\beta)$ . This fact should be noted for evaluation of the liquefaction potential at certain points, since it is fairly difficult to obtain accurate estimates of relative density from in-situ tests.

Figures 4.2(a) and 4.2(b) illustrate the root-mean-squares of the stress and the stress rate distributions normalized by the mean of the maximum velocity at the ground surface. It is apparent that the normalized distributions are approximately expressed by unique curves, with the stress rate having a somewhat wider scatter. For this example, the layer properties are assumed as given in Figure 3.2 and the non-linearity of the soil is included. The results show that the normalized distributions have no relationship with the epicentral distance. Therefore, the stress and stress rate distributions can be calculated easily once the normalized curves are given, i.e., by multiplying the normalized curves by the mean of the maximum velocity.

As an example application of the fatigue theory to the liquefaction phenomenon, the expected cumulative damage per unit of time,  $E[D]$ , is calculated and is shown in Figure 4.3. In this analyses, the stationarity of the stress response is assumed, and the total damage of the surficial ground is obtained by multiplying the duration  $T$  by these results. The surficial ground model analyzed is the same as that in Figure 3.2 but ground water levels are assumed to be 0.5, 1.0 and 2.0m and  $\epsilon$  is assumed to be 0.8. It can be observed that as the water level becomes deeper the sand layer becomes more resistant against liquefaction failure. The sand layer with the ground water level of 2.0m appears to be two times safer than that with the ground water level of 0.5m for the same duration of time. This result is easily verified by recalling that  $E[D]$  is inversely proportional to  $(\frac{1}{\beta})$ th power of  $p_v'$  as given in Equation (4.5). Therefore, once the distribution of  $E[D]$  for a certain ground water level is given,  $E[D]$  for other ground water levels is easily obtained by using the appropriate proportionality factor.

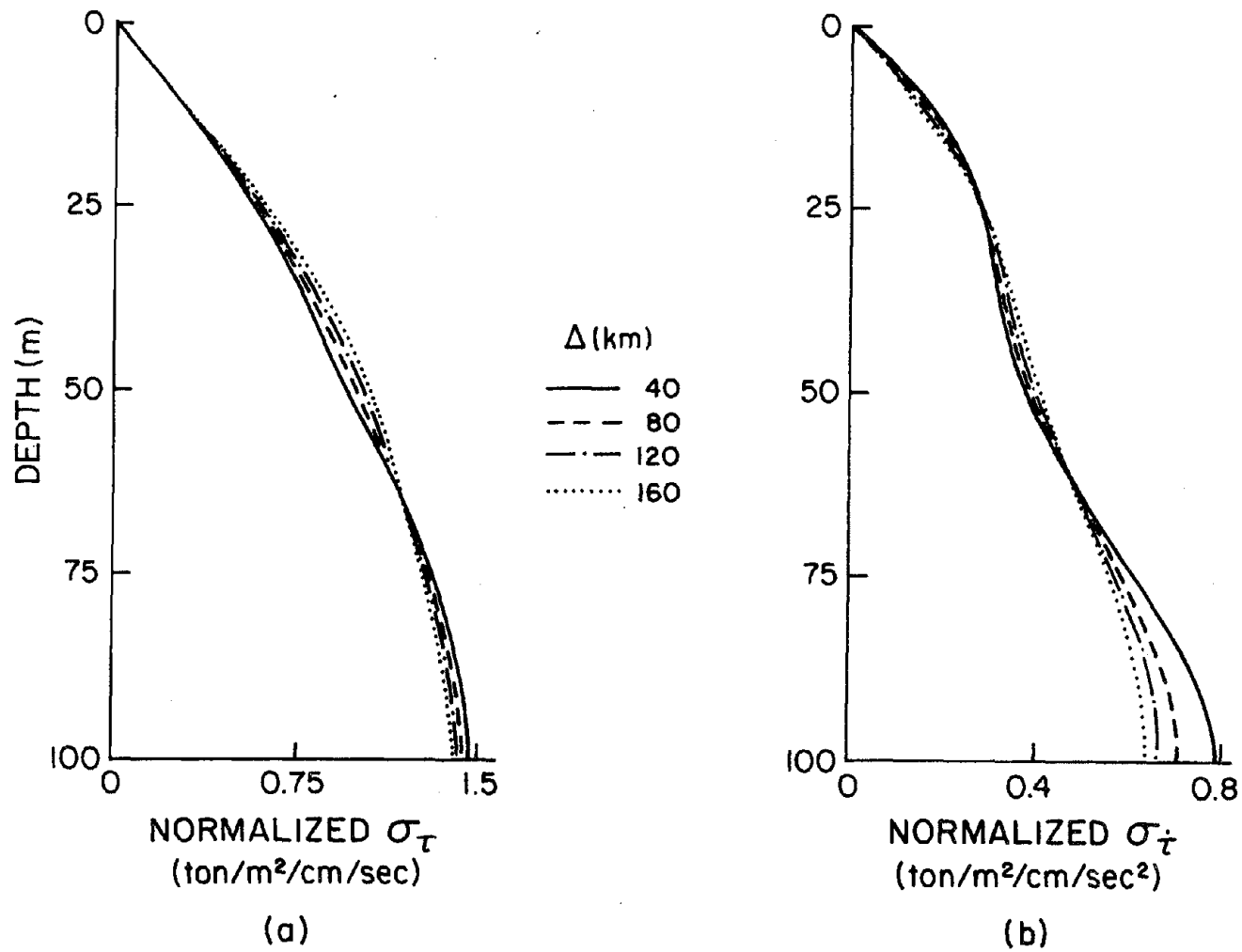


**Figure 4.2** Distributions of root-mean-squares of (a) shear stress,  $\sigma_{\tau}$ , and (b) shear stress rate,  $\sigma_{\dot{\tau}}$ , as normalized by mean peak velocity at ground surface;  $M=7$

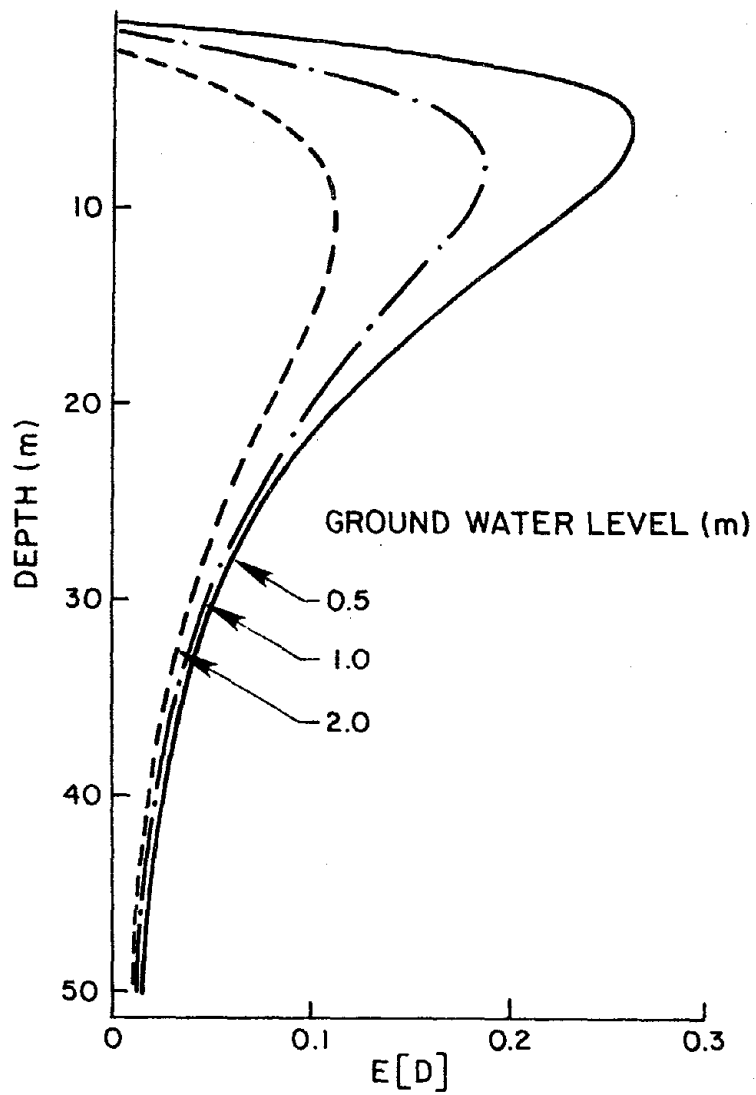


Figure 4.3 Expected cumulative damage per unit time;  $\Delta=40\text{km}$ ,  $M=7$

## 5. APPLICATION TO SEISMIC RISK ANALYSIS OF LIFELINE NETWORKS

Seismic safety analysis of lifeline systems involves reliability assessment of a network of structural systems subjected to earthquakes. Due to high redundancy of lifeline systems, a network reliability analysis in addition to structural reliability is required for the safety assessment. Of particular interest are lifelines of underground piping systems such as water distribution networks. Such buried lifeline systems have the following characteristics which are not seen in ordinary structures. (i) These lifeline systems are buried near the ground surface and are spread over a vast area in which the local geological environment is varied from one place to another. This is important since earthquake intensity is strongly affected by the local geological nature. (ii) In such systems pipes with different diameters and shapes are connected through various joint. As a result, it is very difficult to determine the overall durability of the system because of its complexity and construction difference among different components within the systems.

There have been several methods for calculating lifeline reliability. Panoussis [21] treated the lifeline as a network system and evaluated the probability of the system functioning after a random earthquake occurrence. Taleb-Agha [22] assumed the inter-independency of failure probability among links and joints and analyzed a more realistic network system. However, as discussed by Barlow, Der Kiureghian and Satyanarayana [23], analysis neglecting the joint probability among links and joints is not appropriate for the estimation of the reliability of lifeline systems. In their works, a new algorithm for calculating the reliability of lifeline networks based on graph theory was proposed by means of a transition distance. Wood used their concept and improved the efficiency of the algorithm thus making it possible to apply to large network systems [24]. The development of this method and its application to an existing water distribution system is presented in Reference 25. The concept of transition distance, which defines the seismic risk potential at a certain site in terms of the distance to the earthquake source, offers a considerable reduction in the enumeration process. In the following section, in order to analyze the effect of local geological environment on the reliability of lifeline systems

subjected to seismic risk, the transition distance including the effect of local geological topography will be formulated.

### 5.1. The Transition Distance

The intensity  $Y$  of seismic motion at a particular site is given through an attenuation law in terms of the earthquake magnitude,  $M$ , the shortest distance to the rupture zone,  $r$ , and the parameters expressing the effect of local geological nature at the site. The general form of this relationship can be expressed by

$$Y = f(M, r, C_k) \quad (k = 1, 2, \dots) \quad (5.1)$$

where  $C_k$  are geological parameters such as the natural frequency of the ground, material properties of soil layer and the depth of the site.

The analytical results for attenuation law obtained in Section 3 are based on the modal analysis; where,  $Y$  is a relative response quantity. When an absolute response quantity is required, Equation (5.1) is modified to

$$Y = F(M, r, C_k) = f_b(M, r) + f_s(M, r, C_k) \quad (5.2)$$

where  $f_b$  is an attenuation law for the base rock motion and  $f_s$  is the attenuation law for the response relative to the base rock motion.

If the buried structural component can sustain a certain magnitude of ground shaking, as expressed by  $Y^*$ , the shortest safe distance between the component and the fault rupture is given by

$$r = F^{-1}(M, C_k, Y^*) \text{ or } f^{-1}(M, C_k, Y^*) \quad (5.3)$$

For liquefaction phenomena, the expectation of the total damage is also a function of the earthquake magnitude,  $M$ , the shortest distance to the rupture zone,  $r$ , and parameters,  $C_k$ ,

$$E[D_T] = F(M, r, C_k) \quad (5.4)$$

The critical safe distance for the risk of liquefaction is obtained by searching the shortest distance under the condition of  $E[D_T] = 1.0$ :

$$r = F^{-1}(M, C_k, 1) \quad (5.5)$$

Thus, the component will fail if the rupture occurs within a distance  $r$  from the component. This distance is defined as the transition distance for the component. The "egg-shaped" envelope of transition distances, as shown in Figure 5.1, is obtained for the component  $ij$  provided there is a smooth monotonic change in the local geological nature along the component. This envelope is known as the "transition boundary" for component  $ij$  and is used in lifeline reliability analysis [25].

## 5.2. Seismic Risk Potential

The transition distance defined in the preceding section is a measure of the seismic risk potential of the structural component, since the component will fail if the rupture falls inside this distance. Here, as an example application, the effect of local geological topography on the transition distance has been studied. A two-layered homogeneous ground model is assumed. The material properties of the layers are shown in Figures 5.2 and 5.3. The upper parts of these figures show the transition distances for a given allowable maximum ground velocity at the surface. Figure 5.2 shows results for the given velocity level  $Y^* = 50\text{cm/sec}$ , which are obtained using Equation (5.2) assuming that the velocity attenuation law for base rock is expressed by the relationship given by McGuire [17]:  $V_m = 5.64 \cdot \exp(0.924M) \cdot (0+25)^{1.202}$ . Figure 5.3 shows results for  $Y^* = 30\text{cm/sec}$ , which are obtained using Equation (5.1) considering only the relative velocity response of the surficial layer to the base rock motion. It is observed that the transition distance drastically changes in the transition area from shallow to deep deposited ground. This observation supports the contention that damage to buried pipes is usually concentrated in such transition areas.

The transition distances are also affected by the earthquake magnitude. The variation in the transition distance is notable along the shallow ground at low earthquake magnitudes. On the contrary it is conspicuous along deeper ground for large magnitudes. In general, low frequency components are predominant in the source spectra of strong ground motions of large magnitude earthquake [26]. Also, the natural frequency of ground becomes smaller as the thickness of surficial ground is increased. Since the intensity of ground shaking is a product of

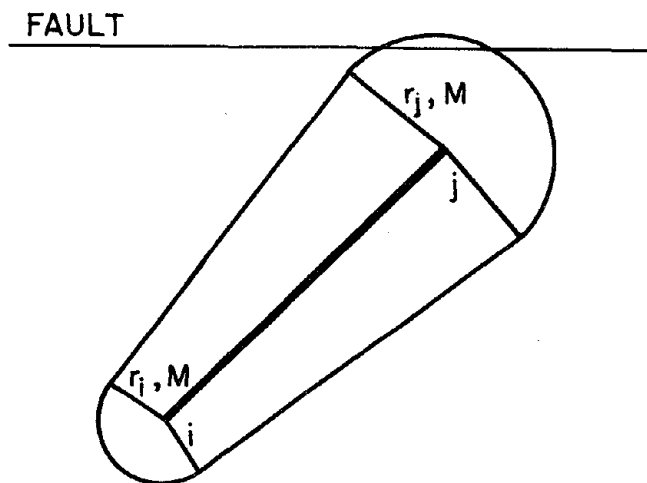
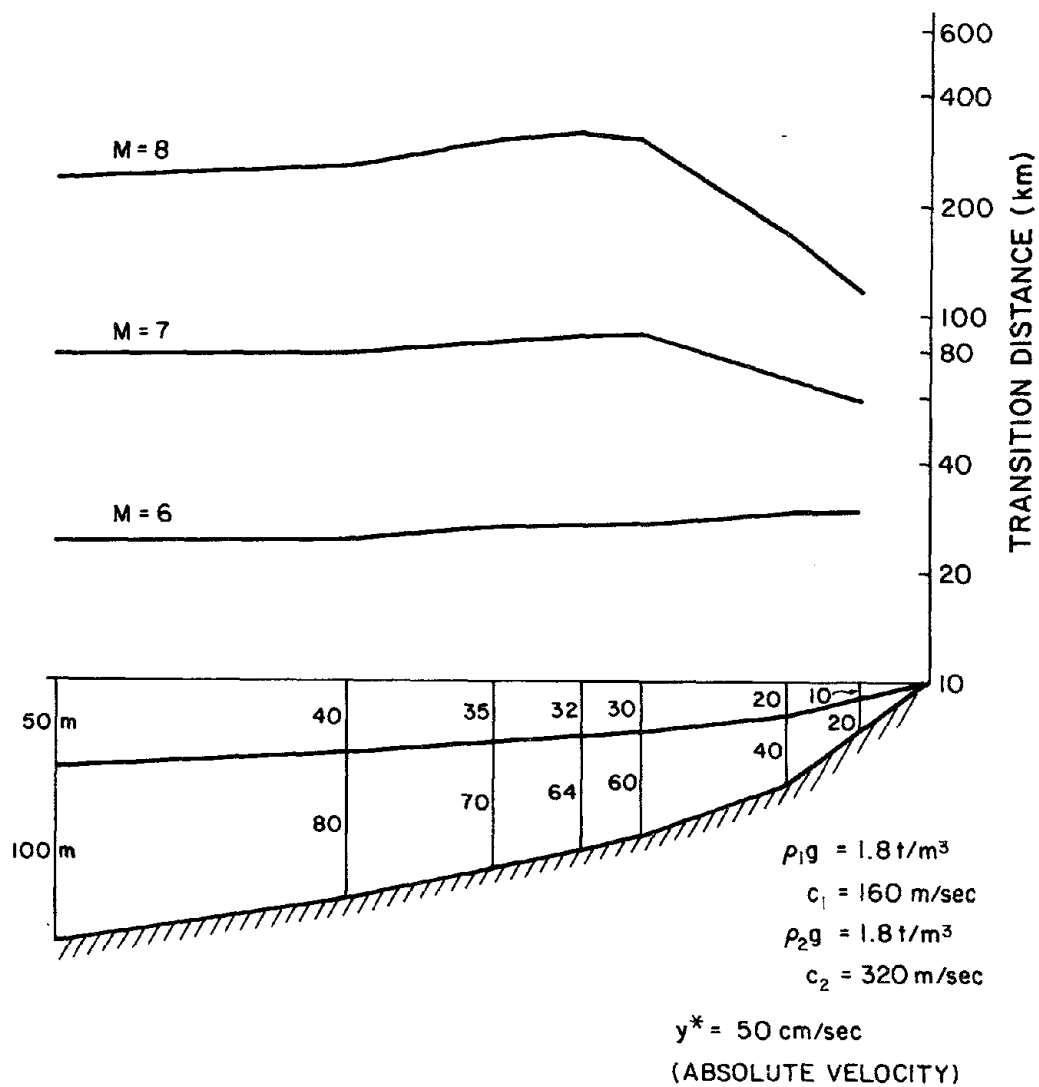
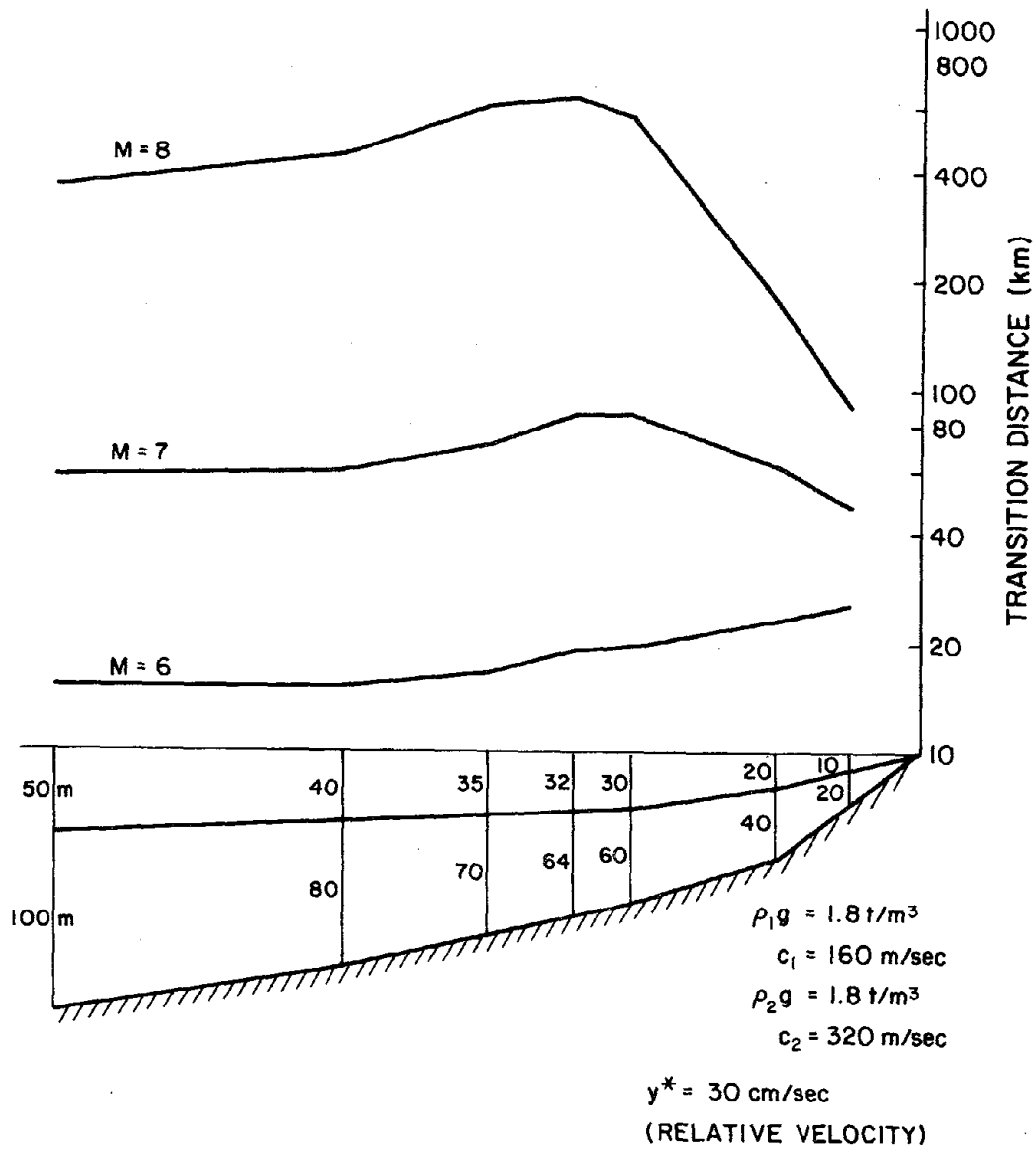


Figure 5.1 Illustration of transition boundary for component  $ij$



**Figure 5.2** Influence of geological topography on transition distance for failure due to absolute velocity



**Figure 5.3** Influence of geological topography on transition distance for failure due to relative velocity

the source spectra and the transfer function of the ground. Larger transition distances are found in deeper surface topography at larger earthquake magnitudes.

Figure 5.4 shows the transition distances for the risk of liquefaction which are also affected strongly by the earthquake magnitude and the geological configuration. The overall view of the transition distances and its variation are almost similar to the case with given allowable velocity amplitude.

To illustrate the compatibility between the calculated transition distances and past liquefaction history, the lower bound of liquefaction history in the relationship between epicentral distance and magnitude are given in Figure 5.5, in which closed circles show previous history of liquefactions [27] and open circles show the results from this analysis. The full and broken lines are the lower bounds for liquefaction for the two sets of data, respectively. There is a somewhat large discrepancy between the two sets of results but the overall agreement is reasonably good.

For analyzing the damage potential to lifeline systems based on the transition distance, the ground structure information is necessary in order to evaluate the dynamic response of the site. The distribution of the shear wave velocity and the density information are essential. However, such information is usually not available for the entire region of a lifeline system. Therefore, one must use a rough estimate based on the classification of soil type. The most common method is to classify the soil as layers of alluvium and diluvium (diluvium is a term used to lump together all pre-Holocene surficial deposits). The information available on the depths of such deposits and reasonable estimates of the shear wave velocities should be sufficient for practical purposes.

The selection of the allowable value,  $Y^*$ , is the next important subject. This value must be given with due consideration to several factors such as: (i) the ground condition, (ii) the buried condition of the pipe, (iii) the material properties of the pipe or the joint, and (iv) the diameter and the thickness of the pipe. A detailed discussion of all these factors is beyond the scope of this report. However, there have been several proposals for this value based on the

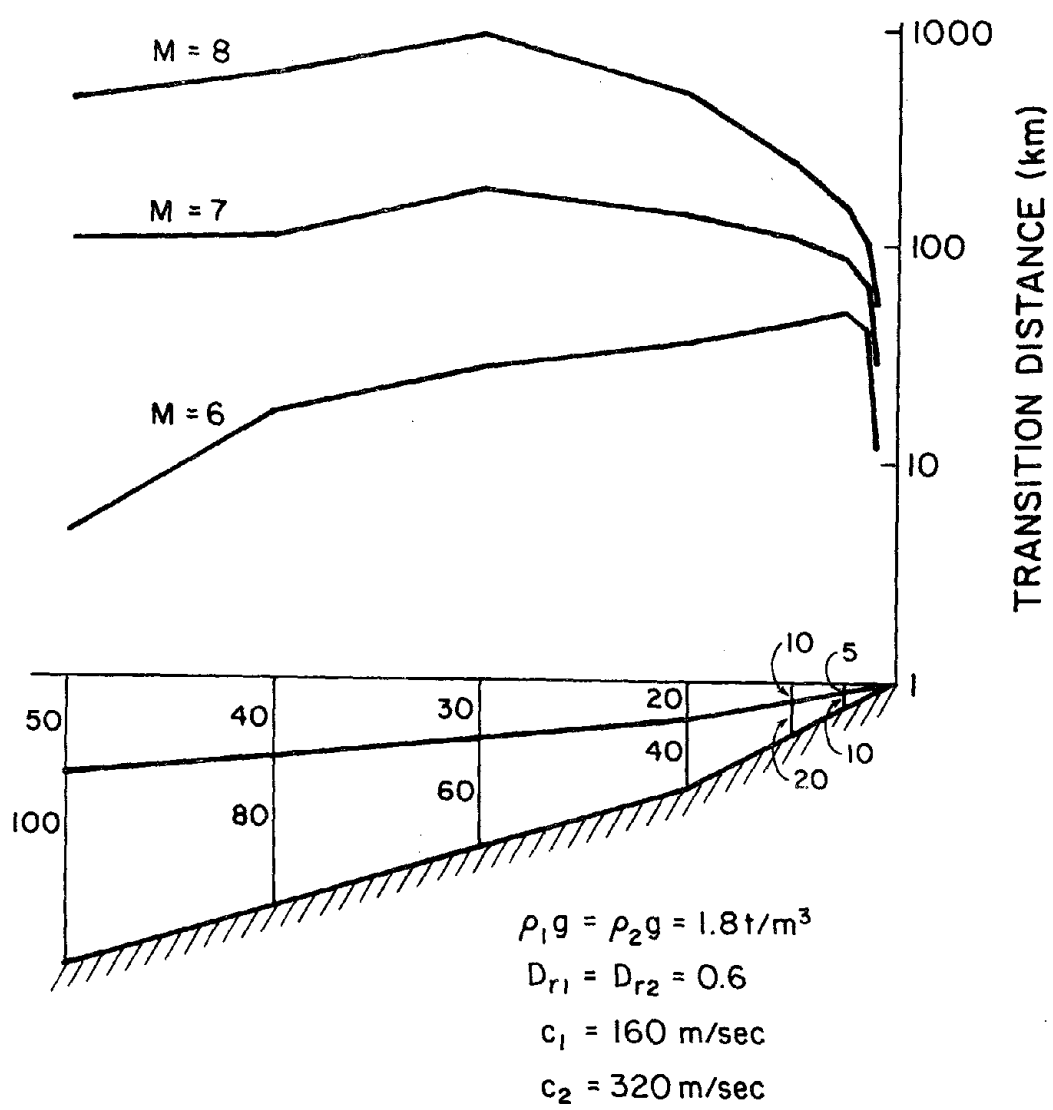
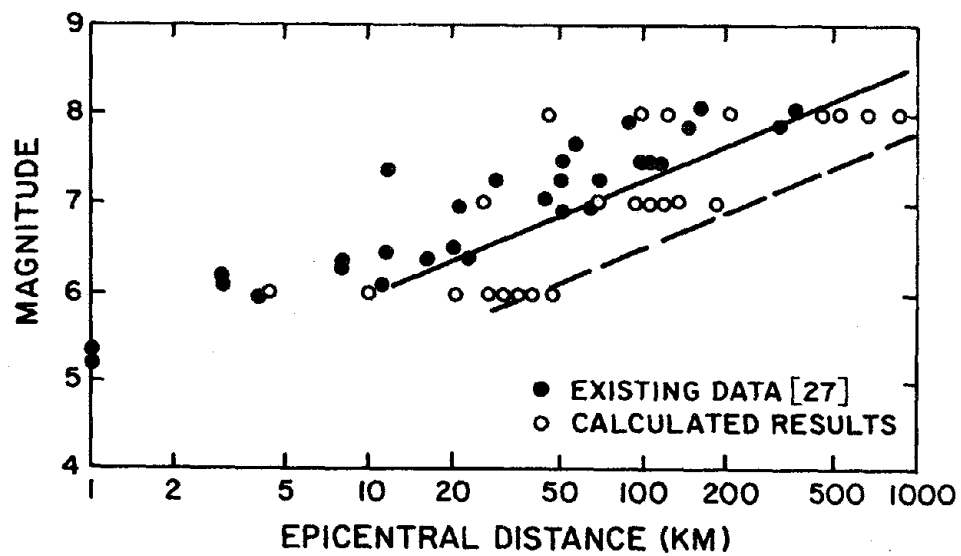


Figure 5.4 Influence of geological topography on transition distance for failure due to liquefaction



**Figure 5.5 Comparison between calculated results and previous history of liquefaction**

actual damage of pipes during earthquakes. Here, based on Toki and Sato's results [28], we have assumed that such damage is strongly related to the magnitude of ground velocity. For design purposes, this allowable velocity must be translated into the amount of stress produced in the pipe, the degree of joints deformation and the bending angle of the joints. The velocity estimation obtained in this report is based on the SH wave propagation theory. Therefore, there are no rational relationships among these factors and the estimated velocity. However, if we can use the magnitude of this velocity as an estimator of the velocity induced by surface waves, then the estimated magnitude can be translated into the strain magnitude divided by the phase velocity. Once the strain magnitude of the freefield is given, the pipe strain and stress, joint deformation and bending angle of the joints may be calculated [29]. A rough estimate of the phase velocity of surface waves may be obtained from the phase velocity at the response mean frequency which appeared in Equation (3.44).

## 6. CONCLUSION

The principal results and conclusions of the present study can be summarized as follows:

1. A theoretical solution has been derived for expressing harmonic waves propagating in sub-surface ground with general inhomogeneity and non-linearity. To take into account the non-linearity of the soil element, the equivalent shear modulus and viscosity have been used. This analysis is a modified application of the multiple reflection theory.
2. The modal superposition method is used to evaluate the intensity of ground shaking during strong earthquake motions. For this purpose, a new iteration scheme for calculating the modal stiffness and damping have been proposed. The method is an extension of the equivalent linearization technique. It has been shown that for several special cases the theoretical solutions assume simple and useful forms. One such solution provides a rational basis for the empirical formula of the fundamental frequency of a soil layer used in practice.
3. A new concept has been proposed for estimating an equivalent modal damping ratio from the non-proportional damping of soil elements taking into consideration the strain dependent non-linearity of soil. It has been observed that the use of the diagonal elements of the coupled damping matrix as the modal damping ratio can lead to gross errors in estimating the equivalent damping ratio especially for higher modes.
4. The relationship between modal damping and epicentral distance has been examined. The results show that the damping ratio is insensitive to the epicentral distance for low frequency modes. Therefore, the assumption of constant, strain-independent modal damping is acceptable for practical purposes. In addition, the damping ratios of high-frequency modes are found to be very high; consequently, modal superposition with first several modes gives considerable accuracy.
5. The stress distribution with depth as normalized by the maximum velocity of ground surface is found to be a measure of response which is not affected by either the inhomogeneity and non-linearity of soil layers or by the epicentral distance. The same result is

also obtained for the stress rate distribution.

6. The fatigue theory is used to analyze the liquefaction phenomenon. It is shown that the accuracy of the relative density and the effective vertical pressure are most important. The second most important term is the stress and least important is the stress rate estimation. The ground water level strongly affects the liquefaction potential.
7. The concept of transition distance has been used to analyze the seismic risk of lifeline systems. This distance is a measure of seismic risk potential for lifeline components. The results obtained indicate that the seismic risk potential drastically changes in the transitional region of the geological structure from shallow to deep soil.

## Appendix

### 1. Derivation of Equation (2.15)

$\lambda(z)$  is derived from infinite products of  $\xi_k$

$$\lambda(z) = \lim_{\Delta h \rightarrow 0} \prod_{k=1}^{j-1} \xi_k \quad (a)$$

when the layer is divided into infinitesimal sub-layers having equal thickness  $\Delta h$ ,  $\xi_k$  is obtained from Equation (2.10) as follows

$$\xi_k = \frac{\beta_k + \beta_{k+1}}{2\beta_{k+1}} = \left( \frac{\beta_k}{\beta_{k+1}} \right)^{1/2} + \frac{1}{8} \left( \frac{\beta'_k}{\beta_k} \right)^2 \Delta h^2 + O(\Delta h) \quad (b)$$

$$\beta'_k = \left. \frac{d\beta(z)}{dz} \right|_{z=k \cdot \Delta h}, \quad \beta_k = \beta(z) \Big|_{z=k \cdot \Delta h}.$$

By substituting Equation (b) into Equation (a), we obtain

$$\lambda(z) = \left( \frac{\beta_1}{\beta_j} \right)^{1/2} + \lim_{\substack{\Delta h \rightarrow 0 \\ j \rightarrow \infty}} \frac{1}{8} \left\{ \left( \frac{\beta'_1}{\beta_2} \right)^2 \Delta h^2 \left( \frac{\beta_2}{\beta_j} \right)^{1/2} + \left( \frac{\beta'_2}{\beta_2} \right)^2 \Delta h^2 \left( \frac{\beta_1}{\beta_2} \right)^{1/2} \left( \frac{\beta_3}{\beta_j} \right)^{1/2} + \dots \right.$$

$$+ \left. \left( \frac{\beta'_k}{\beta_k} \right)^2 \Delta h^2 \left( \frac{\beta_1}{\beta_k} \right)^{1/2} \left( \frac{\beta_{k+1}}{\beta_j} \right)^{1/2} + \dots \right.$$

$$\left. + \left( \frac{\beta'_{j-1}}{\beta_{j-1}} \right)^2 \Delta h^2 \left( \frac{\beta_1}{\beta_{j-1}} \right)^{1/2} + O(\Delta h) \right\}.$$

Then,  $\lambda(z)$  satisfies the following inequality

$$\left| \lambda(z) - \left( \frac{\beta_1}{\beta_j} \right)^{1/2} \right| \leq |A| \frac{H^2}{n} \frac{j-1}{n} + |O(\Delta h)| \quad (c)$$

where  $\Delta h$  is replaced by  $H/n$ ,  $H$  is the thickness of the layer and  $n$  is the number of subdivisions and

$$|A| = \max_{1 \leq k \leq j-1} \frac{1}{8} \left| \left( \frac{\beta'_k}{\beta_k} \right)^2 \left( \frac{\beta_1}{\beta_k} \right)^{1/2} \left( \frac{\beta_{k+1}}{\beta_j} \right)^{1/2} \right|.$$

By increasing the number of subdivisions,  $H^2/n$  becomes smaller and smaller, Equation (c) in the limit yields

$$\lambda(z) = \left\{ \frac{\beta(0)}{\beta(z)} \right\}^{1/2}. \quad (d)$$

## 2. Derivation of $\kappa(z)$

$\kappa(z) dz$  is defined by  $\lim_{\Delta h \rightarrow 0} \eta_{k-1}$  in which

$$\eta_{k-1} = \frac{\beta_k - \beta_{k-1}}{2\beta_k}. \quad (e)$$

The differentiation of  $\beta(z)$  with respect to  $z$  gives

$$\beta_{k-1} = \beta_k - \beta'_k \Delta h + O(\Delta h). \quad (f)$$

By substituting Equation (f) in Equation (e) and taking the limit  $\Delta h \rightarrow 0$ ,  $\kappa(z)$  is given as follows

$$\kappa(z) = \frac{1}{2\beta(z)} \frac{d\beta(z)}{dz}. \quad (g)$$

## REFERENCES

- [1] Chen, P.J., "Growth and Decay of Waves in Solids," *Hundbuch der Physik*, Springer-Verlag, VIa/3. pp. 303-401, (1973).
- [2] Caughey, T.K. "Forced Oscillations of a Semi-Infinite Rod Exhibiting Weak Bilinear Hysteresis," *Journal of Applied Mechanics*, pp. 644-648, (1960).
- [3] Constitutive Relations, *Proceedings of the Tenth International Conference on Soil Mechanics and Foundation Engineering*, Speciality Session 10, (1977).
- [4] Ishihara, K., "Factoring Affecting Dynamic Properties of Soils," *Proceedings of the Fourth Asian Regional Conference on Soil Mechanics and Foundation Engineering*, Vol. 2, pp. 87-100, (July 1972).
- [5] Seed, H.B., "Evaluation of Soil Liquefaction Effects on Level Ground During Earthquake," *Liquefaction Problems in Geotechnical Engineering*, *Proceedings of American Society of Civil Engineers National Convention*, pp. 1-104, (October 1976).
- [6] Finn, W.D.L., K.W. Lee and G.R. Martine, "An Effective Stress Model for Liquefaction," *Proceeding of the American Society of Civil Engineers*, Vol. 130, GT6, pp. 517-533, (1977).
- [7] Ghaboussi, J. and S. U. Dikman, "Analysis of Horizontally Layered Sands," *Proceeding of the American Society of Civil Engineers*, Vol. 104, GT3, pp. 343-356, (1978).
- [8] Sato, T., T. Shibata and I. Ryoji, "Dynamic Behaviour and Liquefaction of Saturated Sandy Soil," *International Symposium on Soils under Cyclic and Transient Loading*, Swansea, pp. 523-532, (January, 1980).
- [9] Donovan, N.C., "A Stochastic Approach to the Seismic Liquefaction Problem," *Proceeding of the First International Conference on Applications of Statistics and Probability to Soil and Structural Engineering*, Hong Kong, (September, 1971).
- [10] Faccioli, E., "A Stochastic Model for Predicting Seismic Failure in a Soil Deposit," *Earthquake Engineering and Structural Dynamic*, Vol. 1, pp. 293-307, (1973).
- [11] Iwasaki, Y.T., "Sand Liquefaction and Its Analysis as Fatigue Phenomenon," *Proceedings of the Fourth Asian Regional Conference on Soil Mechanics and Foundation Engineering*, Vol. 2, pp. 167-171, (July, 1972).
- [12] Der Kiureghian, A., "A Response Spectrum Method for Random Vibrations Analysis of MDF Systems," *Earthquake Engineering and Structural Dynamics* Vol. 9, No. 5, pp. 419-435, (September-October 1981).
- [13] Hardin, B.O. and V.P. Drenovich, "Shear Modulus and Damping in Soils Design Equation and Curves," *Proceeding of the American Society of Civil Engineers*, Vol. 98, SM7, pp. 667-692, (1972).
- [14] Liu, S.-C., Discussion of "Equivalent Viscous Damping for Yielding Structures," by P.C. Jennings, *Proceeding of the American Society of Civil Engineers*, Vol. 94, EM.4, pp. 1003-1008, (1968).
- [15] Kabori, T. and R. Minai, "Linearization Technique for Evaluating the Elasto-Plastic Response of A Structural System to Non-Stationary Random Excitation," *Annual Report of the Disaster Prevention Research Institute*, Kyoto University, No. 10A, pp. 235-260, (1967).
- [16] Cartwright, D.E. and M.S. Longuet-Higgins, "The Statistical Distribution of the Maxima of a Random Function," *Proceeding of the Royal Statistical Society*, Series A, Vol. 237, pp. 212-232, (1956).
- [17] McGuire, R.K., "Seismic Structural Response Risk Analysis, Incorporating Peak Regressions on Earthquake magnitude and Distance," R74-51, Department of Civil Engineering, Massachusetts Institute of Technology, (August 1974).

- [18] Iwasaki, T. and T. Katayama, "Statistical Analysis of Strong-Motion Earthquake Response Spectra," *Proceeding of the United States-Japan Seminar on Earthquake Engineering Research with Emphasis on Lifeline System*, Tokyo, (1976).
- [19] Peacock, W.H. and H.B. Seed, "Sand Liquefaction Under Cyclic Loading Simple Shear Conditions," *Proceeding of the American Society of Civil Engineers*, Vol. 94, SM3, pp. 689-708, (1968).
- [20] Miles, J.W., "On Structural Fatigue Under Random Loading," *Journal of Aeronautical Society*, Vol. 21, pp. 753-762, (1954).
- [21] Panoussis, G., "Seismic Reliability of Lifeline Networks," R74-57, Department of Civil Engineering, Massachusetts Institute of Technology, (September, 1974).
- [22] Taleb-Agha, G., "Seismic Risk Analysis of Lifeline Networks," R75-49, Department of Civil Engineering, Massachusetts Institute of Technology, (December 1975).
- [23] Barlow, R.E., A. Der Kiureghian and A. Satyanarayana, "New Methodologies for Analyzing Pipeline and Other Lifeline Networks Relative to Seismic Risk," *Proceedings of American Society of Mechanical Engineers at the Century 2 Pressure Vessels and Piping Conference*, San Francisco, California, (August 12-15, 1980).
- [24] Wood, R.K., "Efficient Calculation of the Reliability of Lifeline Networks Subject to Seismic Risk," ORC 80-13, Operations Research Center, University of California, Berkeley, (June, 1980).
- [25] Moghtaderizadeh, M., R.K. Wood, A. Der Kiureghian, R.E. Barlow and T. Sato, "Seismic Reliability of Flow and Communication Networks," *Proceedings, Second ASCE/TCLEE Speciality Conference on Lifeline Earthquake Engineering*, Oakland, California, (August, 1981).
- [26] Geller, R.J., "Scaling Relations for Earthquake Source Parameters and Magnitude," *Bulletin of the Seismological Society of America*, Vol. 66, No. 5, pp. 1501-1523, (October, 1976).
- [27] Kuribayashi, E. and F. Tatsuoka, "Brief Review of Liquefaction During Earthquake in Japan," *Soils and Foundations*, Japanese Society of Soil Mechanics and Foundation Engineering, Vol. 15, No. 4, pp. 81-92, (December, 1975).
- [28] Toki, T. and T. Sato, "Estimation of Damage of Water Distribution System by Earthquake," *Recent Advances in Lifeline Earthquake Engineering in Japan*, PVP-43, American Society of Mechanical Engineers, pp. 89-96, (August, 1980).
- [29] Shinozuka, M. and T. Koike, "Estimation of Structural Strains in Underground Lifeline Pipes," *Lifeline Earthquake Engineering--Buried Pipelines, Seismic Risk, and Instrumentation*, Edited by T. Ariman, S.C. Liu and R.E. Nickell, ASME, pp. 31-48, (1979).

## EARTHQUAKE ENGINEERING RESEARCH CENTER REPORTS

NOTE: Numbers in parenthesis are Accession Numbers assigned by the National Technical Information Service; these are followed by a price code. Copies of the reports may be ordered from the National Technical Information Service, 5285 Port Royal Road, Springfield, Virginia, 22161. Accession Numbers should be quoted on orders for reports (PB-----) and remittance must accompany each order. Reports without this information were not available at time of printing. Upon request, EERC will mail inquirers this information when it becomes available.

- EERC 76-1 "Strength and Ductility Evaluation of Existing Low-Rise Reinforced Concrete Buildings - Screening Method," by T. Okada and B. Bresler - 1976 (PB 257 906)A11
- EERC 76-2 "Experimental and Analytical Studies on the Hysteretic Behavior of Reinforced Concrete Rectangular and T-Beams," by S.-Y.M. Ma, E.P. Popov and V.V. Bertero - 1976 (PB 260 843)A12
- EERC 76-3 "Dynamic Behavior of a Multistory Triangular-Shaped Building," by J. Petrovski, R.M. Stephen, E. Gartenbaum and J.G. Bouwkamp - 1976 (PB 273 279)A07
- EERC 76-4 "Earthquake Induced Deformations of Earth Dams," by N. Serff, H.B. Seed, F.I. Makdisi & C.-Y. Chang - 1976 (PB 292 065)A08
- EERC 76-5 "Analysis and Design of Tube-Type Tall Building Structures," by H. de Clercq and G.H. Powell - 1976 (PB 252 220)A10
- EERC 76-6 "Time and Frequency Domain Analysis of Three-Dimensional Ground Motions, San Fernando Earthquake," by T. Kubo and J. Penzien (PB 260 556)A11
- EERC 76-7 "Expected Performance of Uniform Building Code Design Masonry Structures," by R.L. Mayes, Y. Omote, S.W. Chen and R.W. Clough - 1976 (PB 270 098)A05
- EERC 76-8 "Cyclic Shear Tests of Masonry Piers, Volume 1 - Test Results," by R.L. Mayes, Y. Omote, R.W. Clough - 1976 (PB 264 424)A06
- EERC 76-9 "A Substructure Method for Earthquake Analysis of Structure - Soil Interaction," by J.A. Gutierrez and A.K. Chopra - 1976 (PB 257 783)A08
- EERC 76-10 "Stabilization of Potentially Liquefiable Sand Deposits using Gravel Drain Systems," by H.B. Seed and J.R. Booker - 1976 (PB 258 820)A04
- EERC 76-11 "Influence of Design and Analysis Assumptions on Computed Inelastic Response of Moderately Tall Frames," by G.H. Powell and D.G. Row - 1976 (PB 271 409)A06
- EERC 76-12 "Sensitivity Analysis for Hysteretic Dynamic Systems: Theory and Applications," by D. Ray, K.S. Pister and E. Polak - 1976 (PB 262 859)A04
- EERC 76-13 "Coupled Lateral Torsional Response of Buildings to Ground Shaking," by C.L. Kan and A.K. Chopra - 1976 (PB 257 907)A09
- EERC 76-14 "Seismic Analyses of the Banco de America," by V.V. Bertero, S.A. Mahin and J.A. Hollings - 1976
- EERC 76-15 "Reinforced Concrete Frame 2: Seismic Testing and Analytical Correlation," by R.W. Clough and J. Gidwani - 1976 (PB 261 323)A08
- EERC 76-16 "Cyclic Shear Tests of Masonry Piers, Volume 2 - Analysis of Test Results," by R.L. Mayes, Y. Omote and R.W. Clough - 1976
- EERC 76-17 "Structural Steel Bracing Systems: Behavior Under Cyclic Loading," by E.P. Popov, K. Takanashi and C.W. Roeder - 1976 (PB 260 715)A05
- EERC 76-18 "Experimental Model Studies on Seismic Response of High Curved Overcrossings," by D. Williams and W.G. Godden - 1976 (PB 269 548)A08
- EERC 76-19 "Effects of Non-Uniform Seismic Disturbances on the Dumbarton Bridge Replacement Structure," by F. Baron and R.E. Hamati - 1976 (PB 282 981)A16
- EERC 76-20 "Investigation of the Inelastic Characteristics of a Single Story Steel Structure Using System Identification and Shaking Table Experiments," by V.C. Matzen and H.D. McNiven - 1976 (PB 258 453)A07
- EERC 76-21 "Capacity of Columns with Splice Imperfections," by E.P. Popov, R.M. Stephen and R. Philbrick - 1976 (PB 260 378)A04
- EERC 76-22 "Response of the Olive View Hospital Main Building during the San Fernando Earthquake," by S. A. Mahin, V.V. Bertero, A.K. Chopra and R. Collins - 1976 (PB 271 425)A14
- EERC 76-23 "A Study on the Major Factors Influencing the Strength of Masonry Prisms," by N.M. Mostaghel, R.L. Mayes, R. W. Clough and S.W. Chen - 1976 (Not published)
- EERC 76-24 "GADPLEA - A Computer Program for the Analysis of Pore Pressure Generation and Dissipation during Cyclic or Earthquake Loading," by J.R. Booker, M.S. Rahman and H.B. Seed - 1976 (PB 263 947)A04
- EERC 76-25 "Seismic Safety Evaluation of a R/C School Building," by B. Bresler and J. Axley - 1976

- EERC 76-26 "Correlative Investigations on Theoretical and Experimental Dynamic Behavior of a Model Bridge Structure," by K. Kawashima and J. Penzien - 1976 (PB 263 388)A11
- EERC 76-27 "Earthquake Response of Coupled Shear Wall Buildings," by T. Srichatrapimuk - 1976 (PB 265 157)A07
- EERC 76-28 "Tensile Capacity of Partial Penetration Welds," by E.P. Popov and R.M. Stephen - 1976 (PB 262 899)A03
- EERC 76-29 "Analysis and Design of Numerical Integration Methods in Structural Dynamics," by H.M. Hilber - 1976 (PB 264 410)A06
- EERC 76-30 "Contribution of a Floor System to the Dynamic Characteristics of Reinforced Concrete Buildings," by L.E. Malik and V.V. Bertero - 1976 (PB 272 247)A13
- EERC 76-31 "The Effects of Seismic Disturbances on the Golden Gate Bridge," by F. Baron, M. Arikan and R.E. Hamati - 1976 (PB 272 279)A09
- EERC 76-32 "Infilled Frames in Earthquake Resistant Construction," by R.E. Klingner and V.V. Bertero - 1976 (PB 265 892)A13
- UCB/EERC-77/01 "PLUSH - A Computer Program for Probabilistic Finite Element Analysis of Seismic Soil-Structure Interaction," by M.P. Romo Organista, J. Lysmer and H.B. Seed - 1977
- UCB/EERC-77/02 "Soil-Structure Interaction Effects at the Humboldt Bay Power Plant in the Ferndale Earthquake of June 7, 1975," by J.E. Valera, H.B. Seed, C.F. Tsai and J. Lysmer - 1977 (PB 265 795)A04
- UCB/EERC-77/03 "Influence of Sample Disturbance on Sand Response to Cyclic Loading," by K. Mori, H.B. Seed and C.K. Chan - 1977 (PB 267 352)A04
- UCB/EERC-77/04 "Seismological Studies of Strong Motion Records," by J. Shoja-Taheri - 1977 (PB 269 655)A10
- UCB/EERC-77/05 "Testing Facility for Coupled-Shear Walls," by L. Li-Hyung, V.V. Bertero and E.P. Popov - 1977
- UCB/EERC-77/06 "Developing Methodologies for Evaluating the Earthquake Safety of Existing Buildings," by No. 1 - B. Bresler; No. 2 - B. Bresler, T. Okada and D. Zisling; No. 3 - T. Okada and B. Bresler; No. 4 - V.V. Bertero and B. Bresler - 1977 (PB 267 354)A08
- UCB/EERC-77/07 "A Literature Survey - Transverse Strength of Masonry Walls," by Y. Omote, R.L. Mayes, S.W. Chen and R.W. Clough - 1977 (PB 277 933)A07
- UCB/EERC-77/08 "DRAIN-TABS: A Computer Program for Inelastic Earthquake Response of Three Dimensional Buildings," by R. Guendelman-Israel and G.H. Powell - 1977 (PB 270 693)A07
- UCB/EERC-77/09 "SUBWALL: A Special Purpose Finite Element Computer Program for Practical Elastic Analysis and Design of Structural Walls with Substructure Option," by D.Q. Le, H. Peterson and E.P. Popov - 1977 (PB 270 567)A05
- UCB/EERC-77/10 "Experimental Evaluation of Seismic Design Methods for Broad Cylindrical Tanks," by D.P. Clough (PB 272 280)A13
- UCB/EERC-77/11 "Earthquake Engineering Research at Berkeley - 1976," - 1977 (PB 273 507)A09
- UCB/EERC-77/12 "Automated Design of Earthquake Resistant Multistory Steel Building Frames," by N.D. Walker, Jr. - 1977 (PB 276 526)A09
- UCB/EERC-77/13 "Concrete Confined by Rectangular Hoops Subjected to Axial Loads," by J. Vallenias, V.V. Bertero and E.P. Popov - 1977 (PB 275 165)A06
- UCB/EERC-77/14 "Seismic Strain Induced in the Ground During Earthquakes," by Y. Sugimura - 1977 (PB 284 201)A04
- UCB/EERC-77/15 "Bond Deterioration under Generalized Loading," by V.V. Bertero, E.P. Popov and S. Viathanatepa - 1977
- UCB/EERC-77/16 "Computer Aided Optimum Design of Ductile Reinforced Concrete Moment Resisting Frames," by S.W. Zagajeski and V.V. Bertero - 1977 (PB 280 137)A07
- UCB/EERC-77/17 "Earthquake Simulation Testing of a Stepping Frame with Energy-Absorbing Devices," by J.M. Kelly and D.F. Tsztoo - 1977 (PB 273 506)A04
- UCB/EERC-77/18 "Inelastic Behavior of Eccentrically Braced Steel Frames under Cyclic Loadings," by C.W. Roeder and E.P. Popov - 1977 (PB 275 528)A15
- UCB/EERC-77/19 "A Simplified Procedure for Estimating Earthquake-Induced Deformations in Dams and Embankments," by F.I. Makdisi and H.B. Seed - 1977 (PB 276 820)A04
- UCB/EERC-77/20 "The Performance of Earth Dams during Earthquakes," by H.B. Seed, F.I. Makdisi and P. de Alba - 1977 (PB 276 821)A04
- UCB/EERC-77/21 "Dynamic Plastic Analysis Using Stress Resultant Finite Element Formulation," by P. Lukkunapvasit and J.M. Kelly - 1977 (PB 275 453)A04
- UCB/EERC-77/22 "Preliminary Experimental Study of Seismic Uplift of a Steel Frame," by R.W. Clough and A.A. Huckelbridge 1977 (PB 278 769)A08